RECONSTRUCTION OF SEA LEVEL CHANGES IN CHANGWAT PHATTHALUNG

Mr. Karn Phountong

A Project Submitted in Partial Fulfillment of the Requirements

for the Degree of Bachelor of Science Program in Geology

Department of Geology, Faculty of Science, Chulalongkorn University

Academic Year 2016

การจำลองการเปลี่ยนแปลงระดับน้ำทะเล บริเวณจังหวัดพัทลุง

นายกาญจน์ เผื่อนทอง

โครงงานนี้เป็นส่วนหนึ่งของการศึกษาตามหลักสูตรปริญญาวิทยาศาสตรบัณฑิต

ภาควิชาธรณีวิทยา คณะวิทยาศาสตร์ จุฬาลงกรณ์มหาวิทยาลัย

ปีการศึกษา 2559

Project Title: RECONSTRUCTION OF SEA LEVEL CHANGES IN CHANGWAT PHATTALUNG

By: Mr. Karn Phountong

Field of Study: Geology

Project Advisor: Akkaneewut Chabangborn, Ph.D.

Project Co-advisor: Paramita Punwong, Ph.D.

Date of Submission.....

Date of Approval.....

.....

(Dr. Akkaneewut Chabangborn)

Project Advisor

.....

(Dr. Paramita Punwong)

Project Co-advisor

##5632702123: MAJOR GEOLOGY

KEYWORDS: PALEOENVIRONMENT; SEA LEVEL CHANGES; HOLOCENE; PHATTHALUNG; THAI-MALAY PENINSULA; RADIOCARBON DATING.

KARN PHOUNTONG: RECONSTRUCTION OF SEA LEVEL CHANGES IN CHANGWAT PHATTHALUNG. ADVISOR: AKKANEEWUT CHABANGBORN, Ph.D., CO-ADVISOR: PARAMITA PUNWONG, Ph.D., 53 pp.

Sea level changes, one of paleoenvironment data, can be reconstructed from lake sediment data. Since Thale Noi, a freshwater lake in Changwat Phatthalung, Eastern of Thai-Malay Peninsula, have been influenced by the sea, core TLN-CP5 from Thale Noi was analyzed to reconstruct a sea level changes model by examined the sedimentology using the physical property of the core, loss on ignition analysis, and particle size analysis, and an age-depth model from AMS ^{14}C dating using BACON program. The geochronology data indicates that the sea level was very high and was covering the area. The sea level was expected to be falling until 8145 – 7979 cal BP. Then, there was a transgression until 7280 – 6958 cal BP. From palynological data, it suggests that the sea level should remained stable between 7980 – 7787 cal BP and 7280 – 6958 cal BP. Finally, since 7280 – 6958 cal BP, there is, again, a regression until present. In addition, palynological data indicates that there also should had a freshwater run-off into the lake since the environment shifted from a mangrove to a freshwater swamp.

Department: Geology Student's Signature .....

Field of Study: Geology Advisor's Signature .....

Academic Year: 2016 Co-advisor's Signature .....

กาญจน์ เผื่อนทอง : การจำลองการเปลี่ยนแปลงระดับน้ำทะเล บริเวณจังหวัดพัทลุง. (RECONSTRUCTION OF SEA LEVEL CHANGES IN CHANGWAT PHATTHALUNG) อ.ที่ปรึกษาโครงงานหลัก : อ.ดร.อัคนีวุธ ชะบางบอน, อ.ที่ปรึกษาโครงงานร่วม : อ.ดร.ปรมิตา พันธ์วงศ์, 53 หน้า.

ข้อมูลการเปลี่ยนแปลงระดับน้ำทะเลเป็นหนึ่งในข้อมูลสภาพแวดล้อมบรรพกาลที่สามารถหาได้จากการศึกษาตะกอนทะเลสาบ ทะเลน้อยเป็นทะเลสาบน้ำจืดตั้งอยู่ในจังหวัดพัทลุง ทางทิศตะวันออกของแหลมไทย-มลายู และได้รับอิทธิพลจากระดับน้ำทะเล ดังนั้นแท่งตะกอน TLN-CP5 จากทะเลน้อย จึงถูกนำมาวิเคราะห์เพื่อจำลองการเปลี่ยนแปลงระดับน้ำทะเลจากข้อมูลทางกายภาพ, มวลที่หายไปจากการเผา, ขนาดตะกอน, และแบบจำลองระหว่างอายุที่ได้จากการหาอายุคาร์บอน-14 และความลึก โดยใช้โปรแกรม BACON ข้อมูลทางธรณีกาลระบุว่าระดับน้ำทะเลในอดีตสูงมากจนท่วมพื้นที่ศึกษาทั้งหมด และเริ่มลดระดับลงจนกระทั่ง 8145 – 7979 cal BP ต่อมาระดับน้ำทะเลเริ่มสูงขึ้นจนกระทั่ง 7383 – 7156 cal BP ข้อมูลทางเรณูวิทยาระบุว่าระดับน้ำทะเลน่าจะคงที่ระหว่าง 7980 –7787 cal BP ถึง 7383 – 7156 cal BP หลังจากนั้นระดับน้ำทะเลเริ่มลดลงอีกครั้งจนถึงปัจจุบัน ข้อมูลทางเรณูวิทยาบ่งชี้ว่าในช่วงนี้น่าจะมีอิทธิผลจากน้ำจืดที่ไหลลงสู่ทะเลสาบ เพราะสภาพแวดล้อมมีการเปลี่ยนแปลงจากป่าชายเลน เป็นป่าพรุน้ำจืด

ภาควิชา ธรณีวิทยา ลายมือชื่อนิสิต .....

สาขาวิชา ธรณีวิทยา ลายมือชื่ออาจารย์ที่ปรึกษาหลัก .....

ปีการศึกษา 2559 ลายมือชื่ออาจารย์ที่ปรึกษาร่วม .....

ACKNOWLEDGEMENT

First of all, I would like to express my sincere gratitude to my advisor, Dr. Akkaneewut Chabangborn, and my co-advisor, Dr. Paramita Punwong from Faculty of Environment and Resource studies, University of Mahidol, for guidance in completing this senior project from the very beginning. Also, I would like to show my gratitude to Dr. Sakonvan Chawchai, for guidance on particle size analysis.

Secondly, I would like to express my great appreciation to Ms. Jiraprapa Niumpan, and Ms. Bunjong Puangtong for guidance and endless help in my geochemical laboratory work. Moreover, a very special gratitude goes to my colleagues, Ms. Wachirasee Suwansukho and Ms. Worakamon Nudnara, for good advices, assistance, and friendship.

Lastly, my appreciation goes to friends in GEO'57 and GEO'59 for their encouragement.

CONTENTS

		Page
ABSTRACT (Thai)		iv
ABSTRACT (English)		v
ACKNOWLEDGEMENT		vi
TABLE OF CONTENTS		vii
LIST OF TABLES		ix
LIST OF FIGURE		x
CHAPTER I	**INTRODUCTION**	1
	Rationale	
	Objective	
	Scope of work	
	Study area	
	Literature review	
CHAPTER II	**METHODOLOGY**	7
	Loss on Ignition analysis (LOI)	
	Particle size distribution analysis (PSD)	
	AMS ^{14}C dating	
	Age-Depth modelling	
CHAPTER III	**RESULTS**	17
	Physical properties	
	LOI	
	PSD	
	^{14}C dating and age-depth model	
CHAPTER IV	**DISCUSSIONS &CONCLUSION**	24
	Sedimentology	
	Palynology	
	Conclusion	

CONTENTS (continue)

Page

REFERENCES..... 31

APPENDICES..... 34

Appendix A Cores location

Appendix B LOI results

Appendix C PSD results

Appendix D ^{14}C dating results

LIST OF TABLES

		Page
Table 1	Cores location	34
Table 2	Raw LOI Results – 79 samples with color scale	36
Table 3	Raw particle size distribution data	44
Table 4	AMS ^{14}C Dating Results	53

LIST OF FIGURES

		Page
Figure 1.1	Location map of the study area through a satellite image, from LANDSAT 8 path: 125 row: 55, which was taken on 20th March 2016. (Modified from https://earthexplorer.usgs.gov/)	4
Figure 1.2	A map showing coring sites in this study (red circle) and Horton et al. (2005) (red rectangle). (Modified from Royal Thai armed forces headquarter, Royal Thai survey department [RTSD], 2000).	5
Figure 2.1	A methodology diagram	7
Figure 2.2	Samples in crucibles (the furnace can hold up to 15 samples at a time)	11
Figure 2.3	Samples must be weight after drying and heating up to 550 ℃ and 950 ℃.	11
Figure 2.4	15 Samples being place in a furnace	12
Figure 2.5	Samples are being treated with 30% H_2O_2 on a heat plate. The bubble is from the reaction, not from boiling.	12
Figure 2.6	A centrifuge machine. It can hold up to 4 tube at a time.	14
Figure 2.7	A sample are being stirred with magnetic stirrer in 5% Calgon to disperse the sediment particle.	14
Figure 2.8	A samples being wet-sieved with a 500 μm mesh to separate macrofossils.	15
Figure 2.9	Macrofossils are being picked using a stereo microscope and forceps.	15
Figure 2.10	Selected samples in beakers before ABA pretreatment method.	16
Figure 2.11	Samples are base washed (ABA pretreatment)	16
Figure 3.1	Lithostratigraphy of core TLN-CP5. Modified from Yoojam (2015)	19
Figure 3.2	The relationship between depth of deposits and LOI	20

LIST OF FIGURES (continue)

		Page
Figure 3.3	A relationship between depth of deposits and volumetric mean particle size (D [4,3])	20
Figure 3.4	^{14}C dating samples in a sedimentary sequence	21
Figure 3.5	A comparison between the age-depth model and the stratigraphy	22
Figure 4.1	A graph compares lithostratigraphy, organic material (%), $CaCO_3$ (%), and particle diameter with depth and calendar age.	27
Figure 4.2	A graph compares mangrove lithostratigraphy, mangrove pollen (%), transition pollen (%), terrestrial pollen (%), and unidentified pollen (%) with depth and calendar age	28
Figure 4.3	A graph compares Figure 4.1 and 4.2. A red line divided sedimentary sequence into 4 sections due to all information. The lowermost section is a regression. The upper section is a transgression. The upper section is a regression. And The uppermost section is a regression and influence of freshwater run-off into the lake.	29
Figure 4.4	A comparison between this study, Horton et al. (2005), and Chaimanee et al. (1986)	30
Figure 5.1	The function of a laser particle sizer (Horiba instrument, n.d.)	42
Figure 5.2	The shape of the particle (Horiba instrument, Inc., n.d.)	42
Figure 5.3	Mode, median, and mean of a non-symmetrical distribution (Horiba instrument, n.d.)	43

LIST OF FIGURES (continue)

Page

Figure 5.4 The relationship between ^{14}C age and calendar age. The histogram in the left side is a normal distribution of $y_j \pm 2$ SD. The histogram below is a distribution of θ. The light grey area is a calibration curve, IntCal09, ± 2 SD (Blaauw and Heegaard, 2012). 50

Figure 5.5 Linear interpolation method. The relationship between calendar age and depth of deposits. A tiny black dot and dash refer to θ_j ± 2 SD. Then, draw a straight line to connect each dot. From Blaauw and Heegaard (2012). 50

Figure 5.6 a chronological ordering Bayesian age-depth model when $\theta_1 > \theta_2 > \theta_3 >$ 110 cal BP. The light grey area is calibration cure ± 1 SD. The horizontal coloured stripes are y_1, y_2, $y_3 \pm 1$ SD. It is noticed that information, which is emphasized by dark grey section, is consider only. The other are not considered because it conflicts with prior condition. From Ibbetson (2011), (Blaauw and Heegaard, 2012). 51

Figure 5.7 Wiggle-matching method. The green line is a calibration curve with error of 2 SD. Black dots and dashes are y_j. ± 2 SD. Both data is being compared to each other to retrieve calendar age. (Blaauw and Heegaard, 2012). 52

CHAPTER I

INTRODUCTION

Rationale

A tremendously development of Thailand in the past 50 years puts the environmental problems to be considered in this soceity. However, the short interval of record makes its difficult to assess environmental changes or to distinguish the sources of problems between the human and natural activities. For this matter, paleoenvironmental information is necessary to comprehen into the past environment that can be use to better understanding recent environmental problems. However, paleoenvironmental study is very pausity in Thailand.

Paleoenvironmental data, e.g. sea-level fluctuation, vegetation and climate changes, can be reconstructed by marine sediment, geomorphology, ice core, lake sediment, etc. Lake sediment is potentially the most popular archive for this kind of study by various reasons. Firstly, lake sediments are generally not disturbed after deposition. This makes their strengthforward stratigraphic sequence followed the law of superposition that the lower strata are older than their overlaid sedimetary layers (REF). In addition, since lake sediments deposit together with various proxies, e.g. diatom, organic matter, and pollen etc., the paleoenvironmental reconstruction which is based of this archive can be independently assessed based on different proxies and rechecked each other.

The sea level changes in the eastern coast of Thailand have been studied by many researcher (e.g., Chaimanee et al., 1986; Horton et al., 2005; Yoojam, 2015) However, the conclusions are still conflicting. Consequently, objective of this study is to clarify the controversy by given more information using different methods.

Objective

1. To study paleoenvironment in term of sea-level changes

Scope of work

In this study, a core TLN-CP5 from Thale Noi, Phatthalung will be studied on the stratigraphy using loss on ignition analysis (LOI), particle size distribution (PSD) using laser diffraction, and dating using radiocarbon dating method to reconstruct a sea-level change model of Phatthalung.

Study area

Thale Noi, which is locatedat 7° 48.65’ N and 100° 7.45’ E, is a freshwater lake in Changwat Phatthalung, the east coast of Thailand (Figure 1.1). Most of Phatthalung area is flat of less than 10 meters above mean sea level (MASL) (Figure 1.1). This study collected the sediment core from Thale Noi. Thale Noi covered the area of about 25 km^2 and has 1 - 2 m water depth. Thale Noi’s water supply is mainly from the long channels in the north, east and west of the lake. Due to recently deforestation, the water inlet has been considered to be significantly decrease compare to the past. The southern part of Thale Noi is connected to the northern part of the Great Songkhla Lake by a 3-km-long-canal, Khlong Nang Riam and a 1-km-long-canal, Khlong Ban Klang (Figure 1.2). The western part of the lake is an undulating area which is approximately 10 – 20 MASL. There are the single mountains (not a range) of Permian Limestone in the south of Thale Noi, and Jurassic-Cretaceous clastic sedimentary rock in the rest. These mountains are less than 100 m high (Chaimanee et al., 1986).

Thale Noi is mainly surrounded by the Quaternary sediments which can be further classified into 3 classes (Chaimanee et al., 1986). Firstly, west of the lake compost of silt beach deposits. Secondly, the lowland marsh deposits have been

found along the lake margin which are mainly composed of dark brown to brownish grey clay with high organic material, interbedded with brownish black peat layer. Finally, clastic sediment deposits are predominance in the lake area.

Thailand's climate is under influence of Inter Tropical Convergence Zone (ITCZ), monsoons, and tropical cyclone (Ministry of Information and Communication Technology, Thai Meteorological Department [TMD] , 2015) Thus, under Köppen climate classification, Phatthalung and most regions in Thailand has under the tropical monsoon climate (Am) which is one of tropical moist climate (A) (TMD, 2015; Ministry of Natural Resources and Environment, Department of Mineral Resources [DMR], 2007; Chaimanee et al., 1986). There are only two season in Southern Thailand i.e. summer and rainy season. In addition, the temperature in this region is mild throughout the year because of the maritime characteristic (TMD, 2015). Rainfalls in the eastern coast of the south Thailand reach their maximum in November to January caused by Northeast monsoon (TMD, 2015).

Considering Thailand's climate factors, firstly, ITCZ usually stays in Southern Thailand in May and October (TMD, 2015). Secondly, there are 2 monsoons throughout the year: SW monsoon in mid-May to mid- October which brings moist, warm air from Indian Ocean, and NE Monsoon in mid-October to mid-February (TMD, 2015). Finally, tropical cyclone is mostly from South China Sea. Its strength is characterized by wind speed into 3 categories: tropical depression (less than 63 km/hr.), tropical storm (between 63 and 118 km/hr.), and typhoon (more than 118 km/hr.) (TMD, 2015)

Great Songkhla Lake, including Thale Noi is in the Satingpra Penisula where is less affected by Southwest monsoon caused by a rain shadow of Nakhon Si Thammarat Range (Stargardt, 1983; Horton, 2005). Most of the precipitation comes from the South China Sea due to strengthen northeast monsoon (Horton et al. 2005).

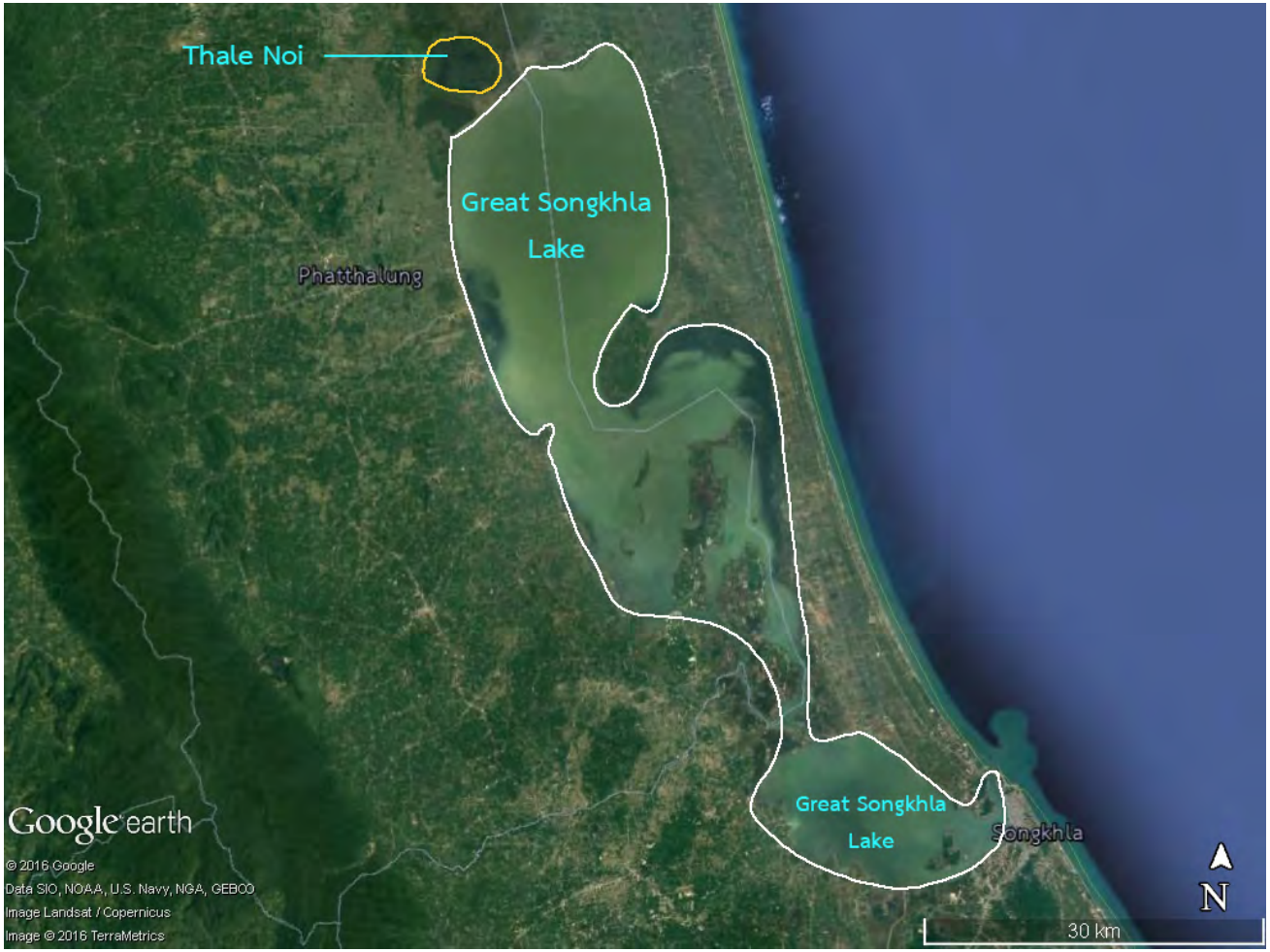

Figure 1.1 Location map of the study area through a satellite image from Google earth, which was taken in 2016. (Modified from https://earthexplorer.usgs.gov/)

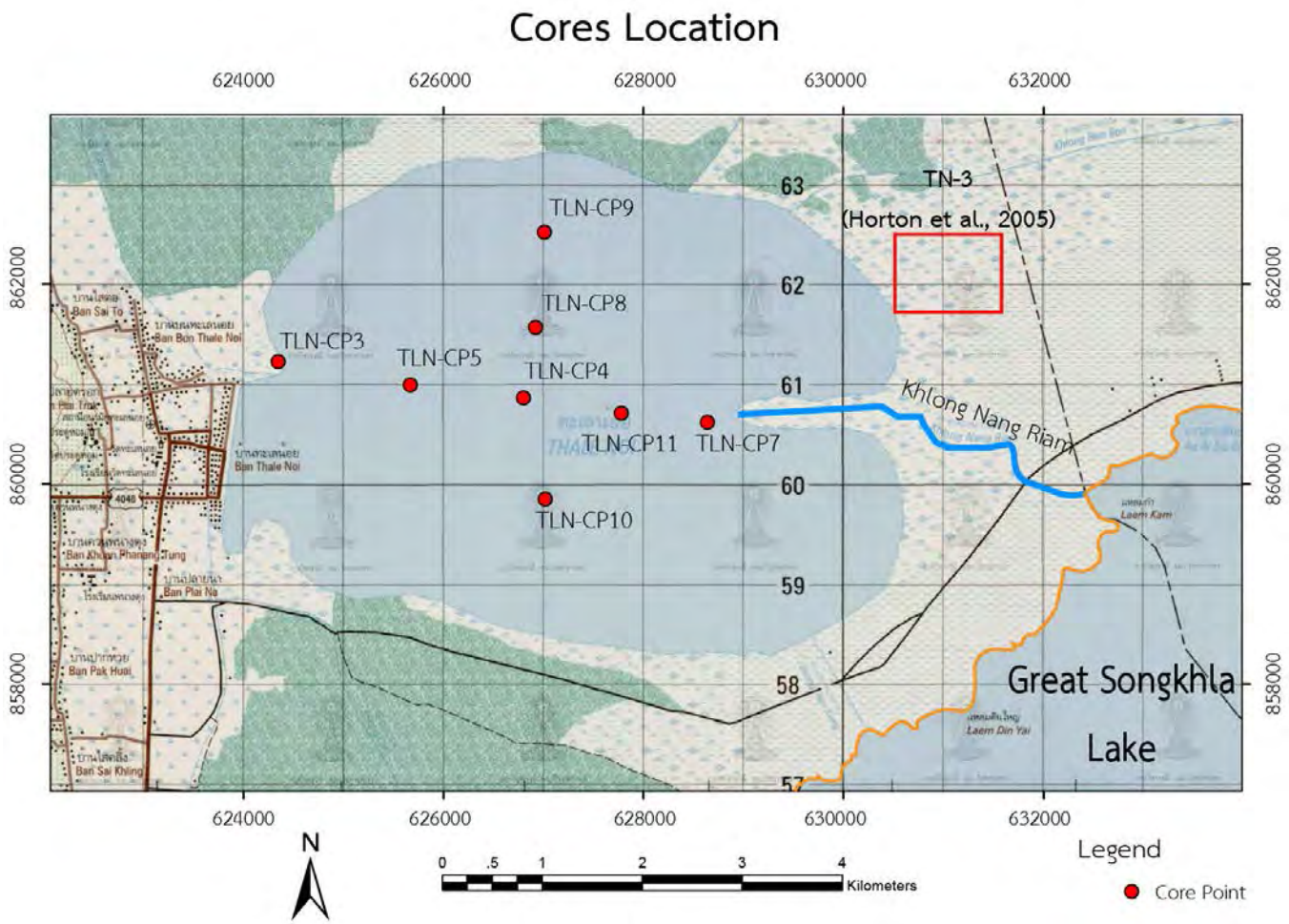

Figure 1.2 A map showing coring sites in this study (red circle) and Horton et al. (2005) (red rectangle). (Modified from Royal Thai armed forces headquarter, Royal Thai survey department [RTSD], 2000).

Literature review

Chaimanee et al. (1986) drilled 201 boreholes using augers: Edelman Auger, Qauge Auger, Suction Corer, and Gut to study Quaternary sediment in the North of Great Songkhla Lake (map sheet: 5024 I and 5024 IV) and also Thale Noi. Regarding to sediment characteristic, and ^{14}C dating, Chaimanee et al. (1986) concluded that this area was a part of Sunda shelf during the late Pleistocene. A transgression had begun between 8090 and 7890 year BP and subsequently followed by a regression between 5890 and 5770 BP.

Horton et al. (2005) reconstructed sea-level fluctuation based on sediment characteristic and palynology in Thale Noi. Since the beginning of Quaternary, the area is presumed to be tectonically stable, with very low vertical crustal movement (c. <0.1 mm/yr) (Tjia, 1996). Lake sediment proxies including geochronological information indicate that sea-level was about 22 m lower than present in the early Holocene. A sea level rise started at about 9700 - 9250 year BP and subsequently reach their highstand at about 4850 – 4450 cal. BP. After that, the sea-level steadily declined of about c. -1.1 mm/yr.

Yoojam (2015) correlated sediment cores derived from Thale Noi. The sediment stratigraphies suggest that Thale Noi consist of two basins. This result corresponds well with Chinanee et al, (1986) that propose mangrove and intertidal environments in the western and eastern part of the lake.

CHAPTER II

METHODOLOGY

The methodology of this study is summarize as follows.

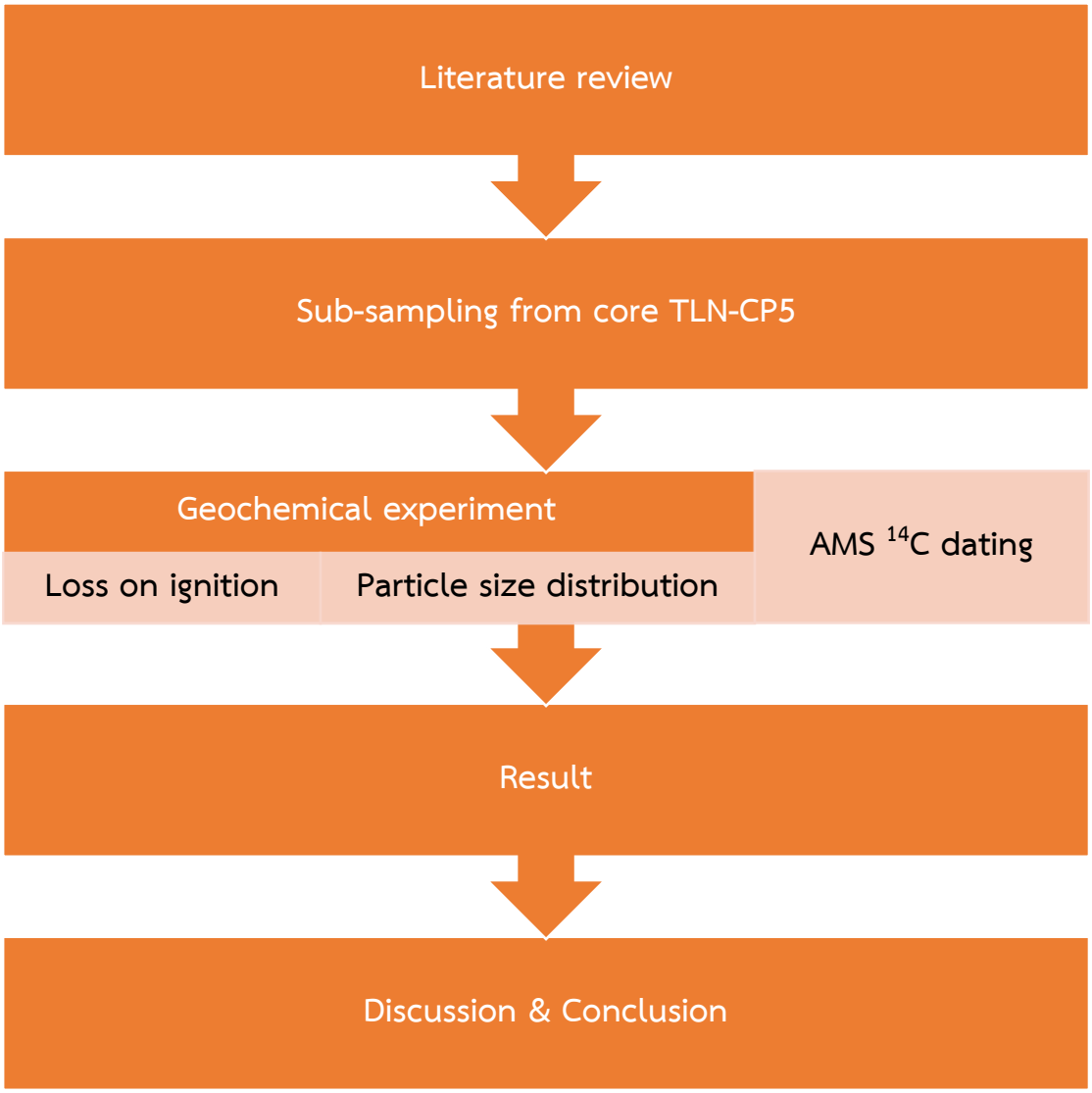

Figure 2.1 A methodology diagram

Sub-sampling

Core TLN-CP5 had already been described, correlated and sub-sampling every 1 cm by Yoojam (2015). In this study, those samples were selected every 5 am and 10 cm to be prepared for loss on ignition (LOI) (detail in Appendix B) and particle size analysis (PSD) (detail in Appendix C), respectively. Moreover, some samples were choosen for AMS radiocarbon dating in regarding to lithostratigraphy (detail in Appendix D).

Geochemical experiment

All the samples which has been selected was proceed in these experiment

1. LOI (based on Heiri et al., 2001)
    3.1 Weigh crucibles and record the value
    3.2 Place samples in the crucible 15 samples (the furnace can only hold up to 15 samples). Weigh them and record the value.
    3.3 Place crucibles in an oven at 105 ℃ overnight to eliminate water content.
    3.4 Take crucibles out of the oven, weigh, and record the value.
    3.5 Place crucibles in a furnace at 550 ℃ for 6 hours to eliminate organic material.
    3.6 Take crucibles out of the furnace, weigh, and record the value.
    3.7 Place crucibles, after heating at 550 ℃, in the furnace at 950 ℃ for 3 hours to eliminate inorganic carbon content in the form of CO_2 gas
    3.8 Take crucibles out of the furnace, weigh, and record the value
    3.9 Repeat No. 1.1 to 1.8 until all samples are dealt with.
    3.10 Calculate LOI_{550} and LOI_{950} using equation 1.1, 1.2, 1.3, and 1.4

2. PSD (based on Rowell, 1994)
    2.1. Place samples in 250 ml beakers
    2.2. Add 10% HCl 20 ml in all beakers inside the hood to eliminate carbonate content.
    2.3. Add 10% H_2O_2 20 ml in all beakers inside the hood to eliminate organic material.
    2.4. Add 30% H_2O_2 in all beakers inside the hood until the reaction does not longer occur.
    2.5. Place beakers on heat plates at 60 – 80 ℃, and add 30% H_2O_2 in all beakers inside the hood until the reaction does not longer occur.
    2.6. Transfer samples from beakers, into test tubes. Then, rinse them with distilled water 3 times.
    2.7. Pour water in the test tube away, and soak the samples with 5% Calgon (Sodium haxametaphosphate) to disperse the particle.
    2.8. Pour samples into vials, label them, and send them to STREC for particle size analysis.

3. AMS ^{14}C Dating (based on Björck and WohlFarth, 2001; Brock et al., 2010)
    3.1 Soak sediment samples in 5% Calgon to disperse clay particles.
    3.2 Wet-sieve samples with a 500 μm mesh to separate macrofossils from the sediment. Macrofossils are larger that 500 μm.
    3.3 Pick macrofossils, which are suitable for AMS ^{14}C dating, for examples, leaves, and woods, using a stereo microscope and forceps and place them in beakers.
    3.4 Place beakers into an oven at 60 ℃ overnight to dry them.
    3.5 Take them out of the oven, and add enough 1 M HCl in all beakers at 80 ℃ for 20 minutes to eliminate carbonate content.

3.6 Rinse them with distilled water 3 times.

3.7 Add enough 0.2 M NaOH in all beakers at 80 °C for 20 minutes to eliminate organic acid.

3.8 Rinse with distilled water 3 times.

3.9 Add enough 1 M HCl in all beakers at 80 °C for an hour to eliminate dissolved atmospheric CO_2 during base wash.

3.10 Rinse with distilled water 3 times.

3.11 Place beakers into an oven at 60 °C to dry them.

3.12 Transfer samples into vials, label them, and sent to DirectAMS, Bothell, WA, USA

Figure 2.2 Samples in crucibles (the furnace can hold up to 15 samples at a time)

Figure 2.3 Samples must be weighed after drying and heating up to 550 °C and 950 °C.

Figure 2.4 15 Samples being place in a furnace

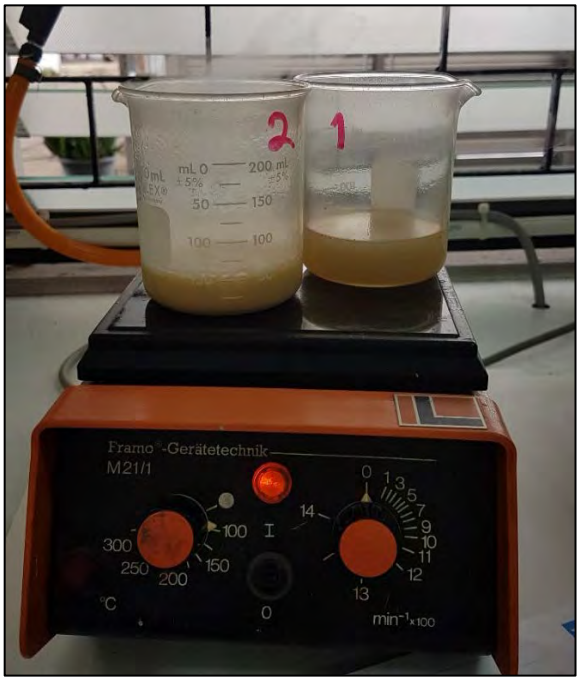

Figure 2.5 Samples are being treated with 30% H_2O_2 on a heat plate. The bubble is from the reaction, not from boiling.

Result

LOI values were used to modify the lithostratigraphy, and presumed to represent organic and inorganic matter contents. Changes in runoff were considered by mean of particle size obtained from PSD.

An age-depth model was constructed based on nine sequently ^{14}C dating results and BACON (Bayesian Accumulation Histories for Deposits) (Blaauw and Christen, 2011). The model consists of calibrated dates distribution using Bayesian approaching and Intcal13 (Reimer et al., 2013), and estimation between dates using autoregressive (AR) gamma process (Blaauw and Christen, 2011).

AR modelling is a linear method of estimating the persistence structure or memory in time-series analysis. In the time series context, this mean that past value of a series is used to estimate its current value (Matthews, 2014)

Discussion and conclusion

Details are in chapter IV.

Figure 2.6 A centrifuge machine. It can hold up to 4 tube at a time.

Figure 2.7 A sample are being stirred with magnetic stirrer in 5% Calgon to disperse the sediment particle.

Figure 2.8 A samples being wet-sieved with a 500 μm mesh to separate macrofossils.

Figure 2.9 Macrofossils are being picked using a stereo microscope and forceps.

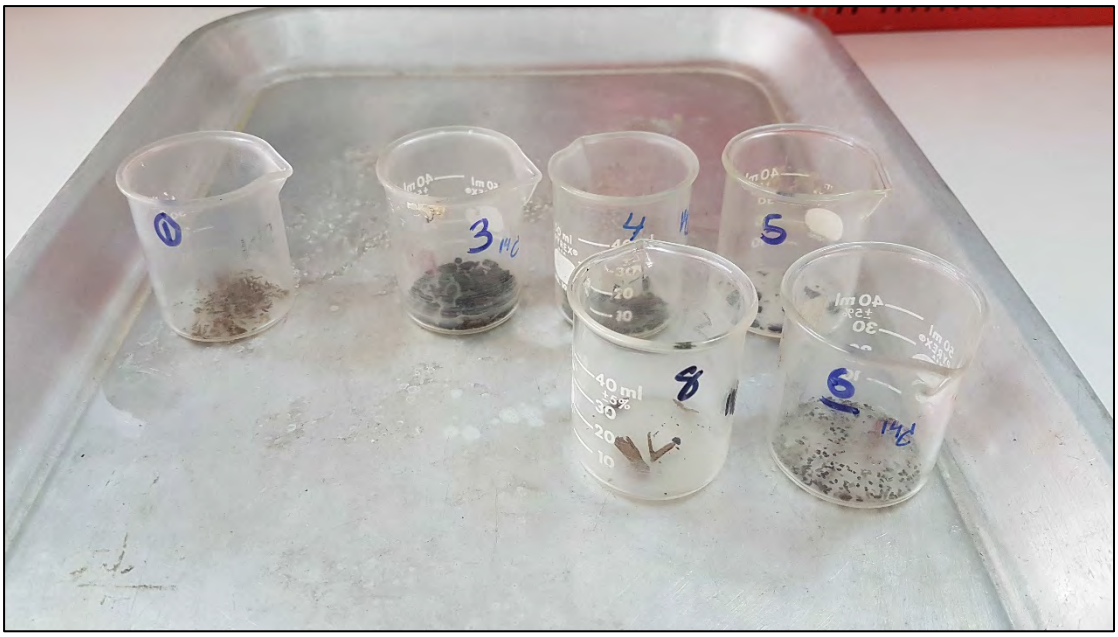

Figure 2.10 Selected samples in beakers before ABA pretreatment method.

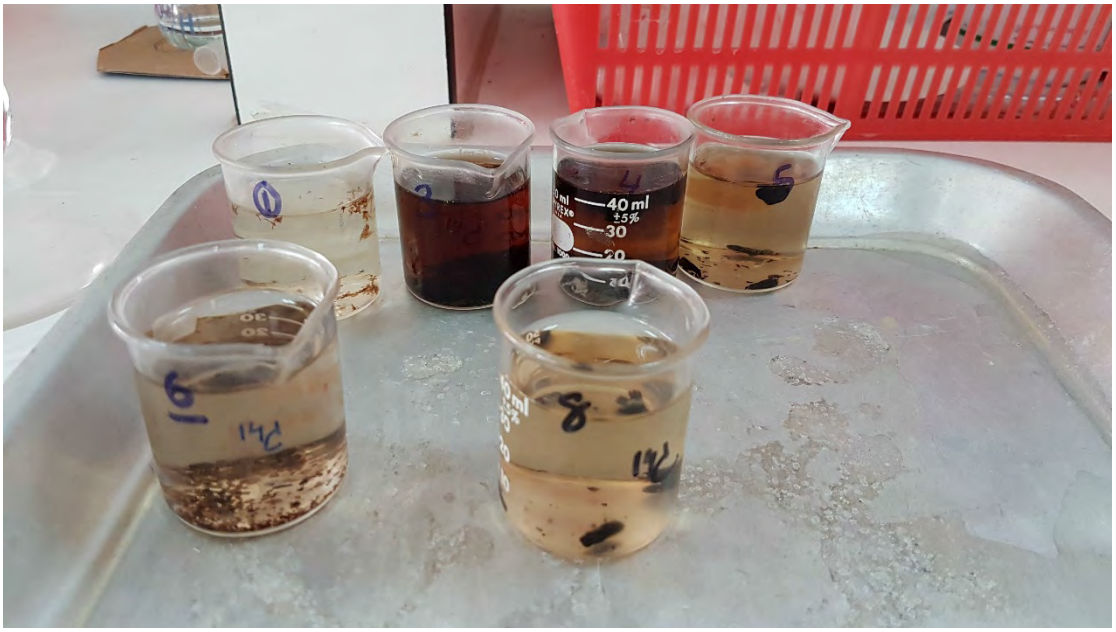

Figure 2.11 Samples are base washed (ABA pretreatment)

CHAPTER III

RESULTS

Physical property

Lithostratigraphy of core TLN-CP5 composes of 5 sedimentary units as follows: stiff clay (unit E: 228.5 – 237.5 cm), dark grey clay (unit D: 194 – 228.5 cm), peat (unit C: 147 – 194 cm), clay with detrital organic matter (unit B: 67 – 147 cm) and gyttja clay (unit A: 0 – 67 cm) (Yoojam, 2016) (Figure 3.1).

Loss on ignition

79 samples were selected for LOI analysis. After that, they were used to reconstruct a relationship between depth vs. % organic carbon content and % carbonate content (Table 2, and Figure 3.2 and 3.3). The variation of % organic carbon content corresponds well with % carbonate content.

LOI at 550 C indicate that % organic carbon contents are a fluctuated between 5 and 15% at approximately 235-190 cm. They remarkably increase to 60 – 90% between 190 and 140 cm, and suddenly decreased to 5% at approximately 40 – 140 cm. In the sedimentary unit A, % organic carbon contents vary from 15 to 30%.

% carbonate contents regarding to LOI 950 C is relatively stable about 5% from 235-190 cm. The contents become increase to about 15% in sedimentary unit C. Despite they gradually decline from 15% at 185 cm to 5% at the core top, the progressive decrease in % carbonate contents are intervened by a layer of low % carbonate contents between 148 and 168 cm.

Particle size analysis

Particle size is about 12.5 μm in sedimentary unit E and D. However, the size varies from 5 to 12.5 μm in sedimentary unit C. In unit B and A, particle size gradual increases from 5 at the bottom of unit B to 14 μm at the top of unit A. There is a peak of particle size at about 120 cm which have been considered to be an error of experiment (Figure 3.4).

Radiocarbon dating and age-depth modelling

The age-depth model has been constructed based on 9 ^{14}C ages and BACON (Blaauw and Christen, 2011). The age of sediment sequence is from 7200 to 8200 cal yr. BP (Figure 3.5 and Figure 3.6). The constant rate of sedimentary deposition can be recognized from 235 to 194 cm. At this point, the bottom of unit B, which can be found as a sharp lower boundary (about 148 cm) in sediment sequence, has been defined a hiatus that suggests non or low deposition rate for about 200 years. The sedimentation rate increases in the lower part of unit B from 148 to 90 cm, and become decrease from 90 to 56 cm. In addition, the dating result of sample obtained from 10 cm from the top defines the recent period.

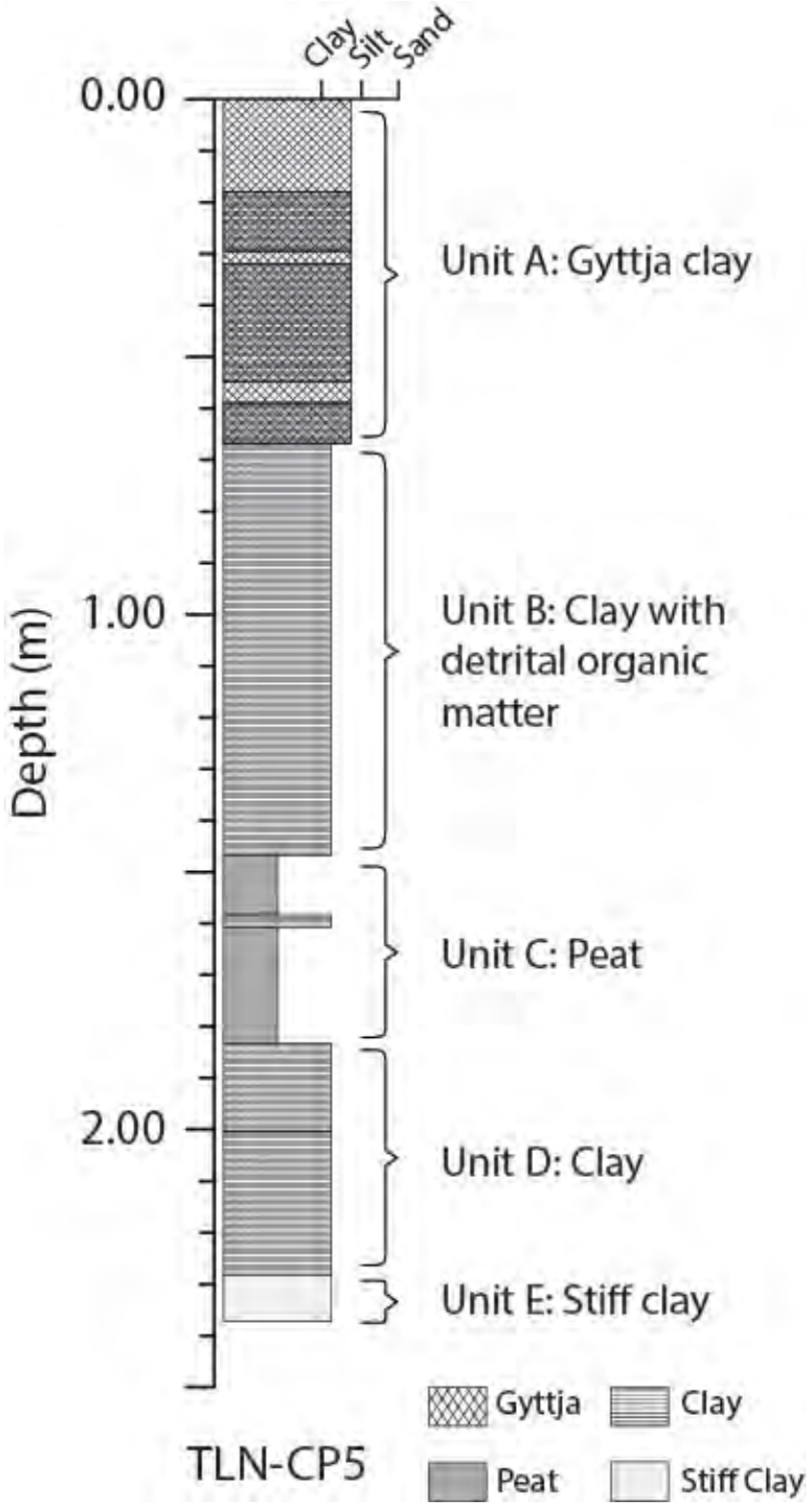

Figure 3.1 Lithostratigraphy of core TLN-CP5. Modified from Yoojam (2015)

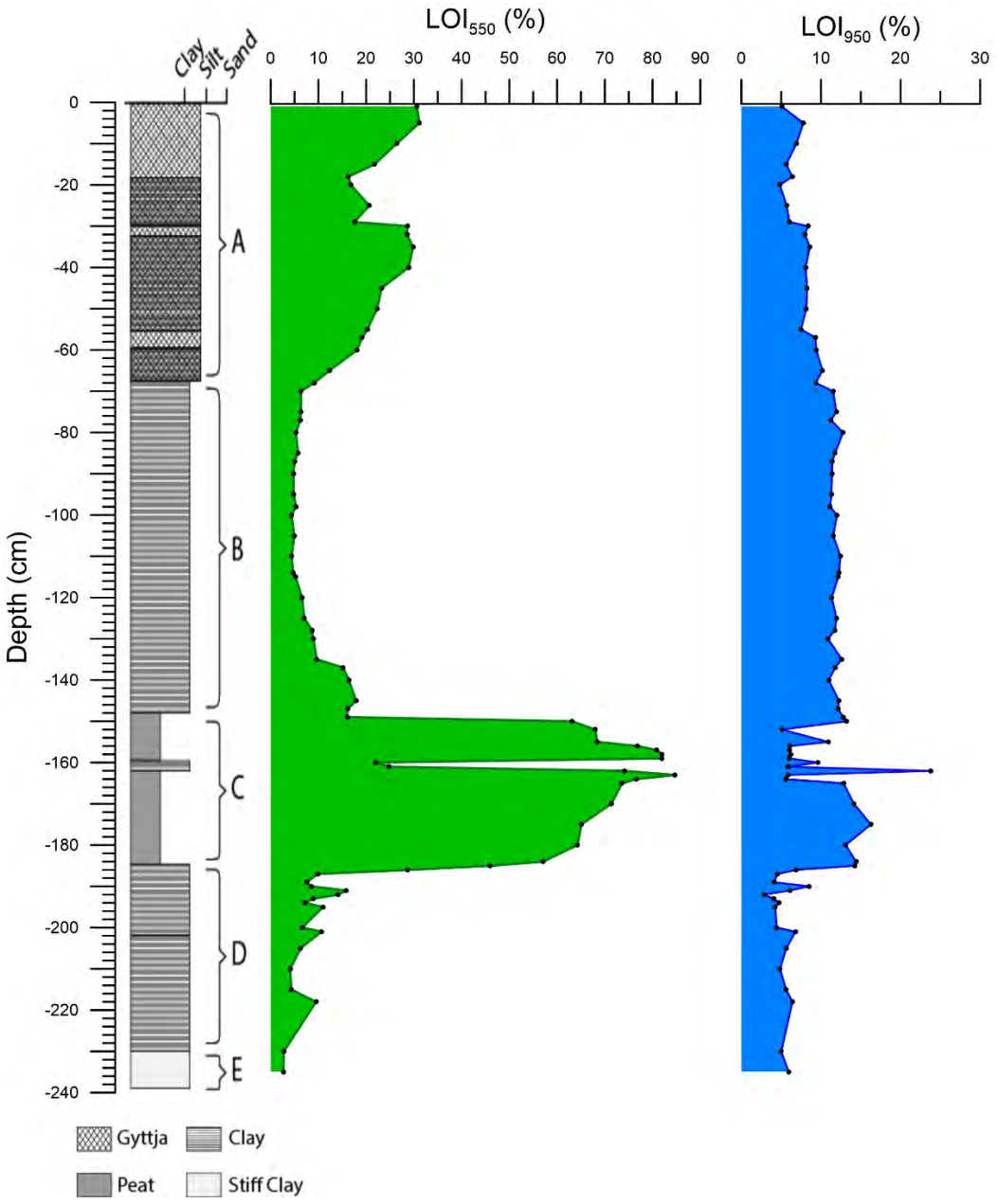

Figure 3.2 The relationship between depth of deposits and LOI

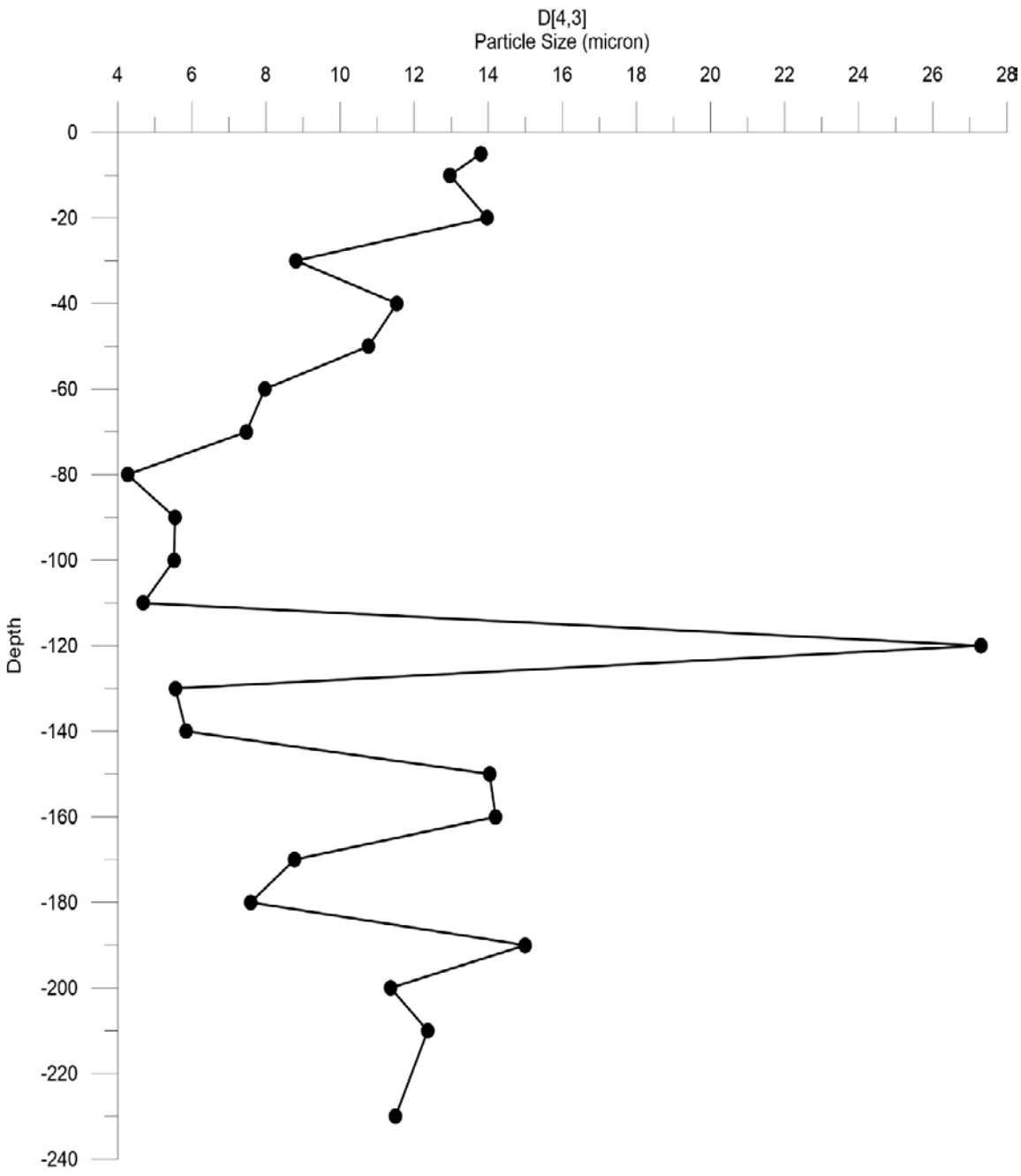

Figure 3.3 A relationship between depth of deposits and volumetric mean particle size (D [4,3])

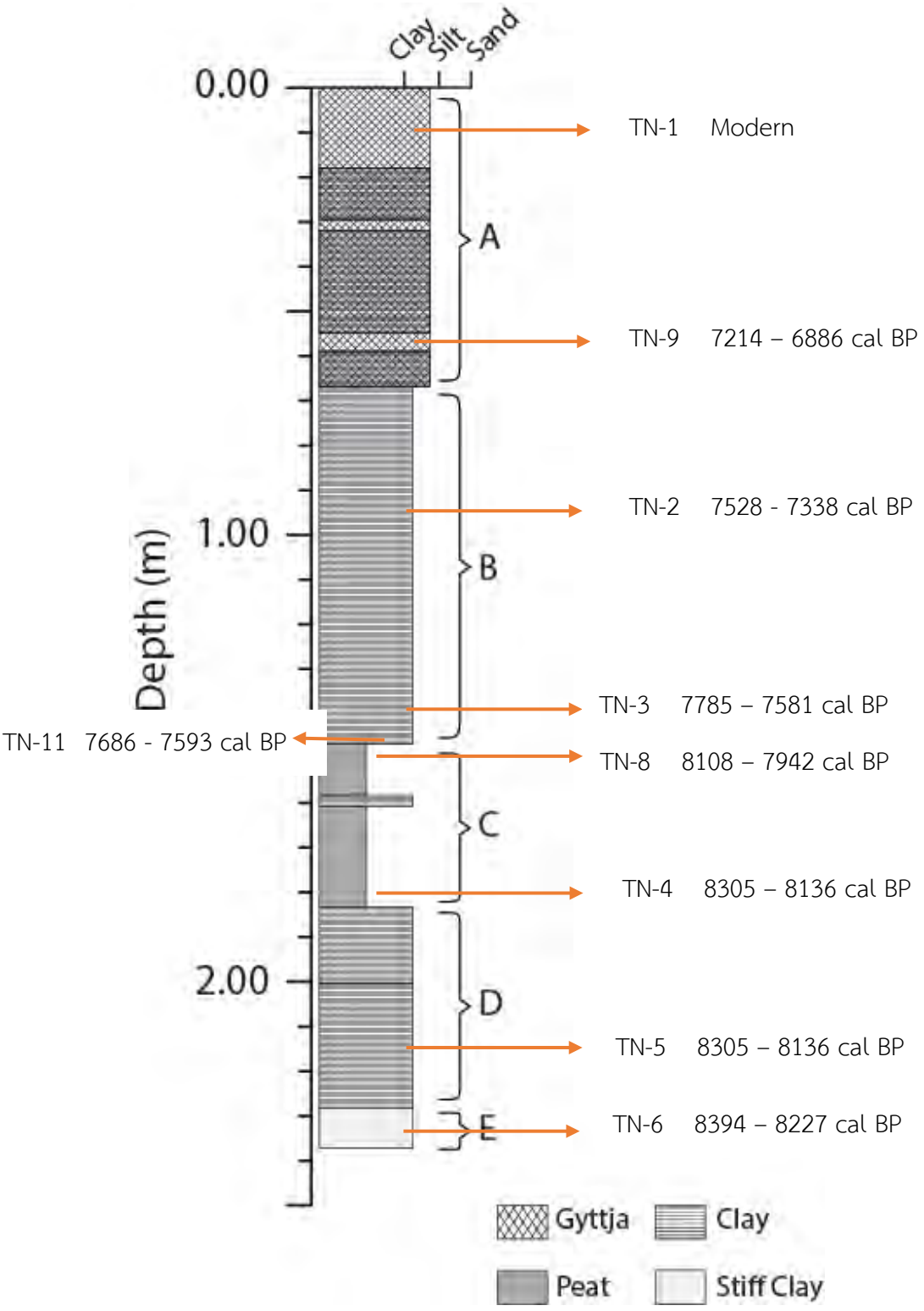

Figure 3.4 ^{14}C dating samples in a sedimentary sequence

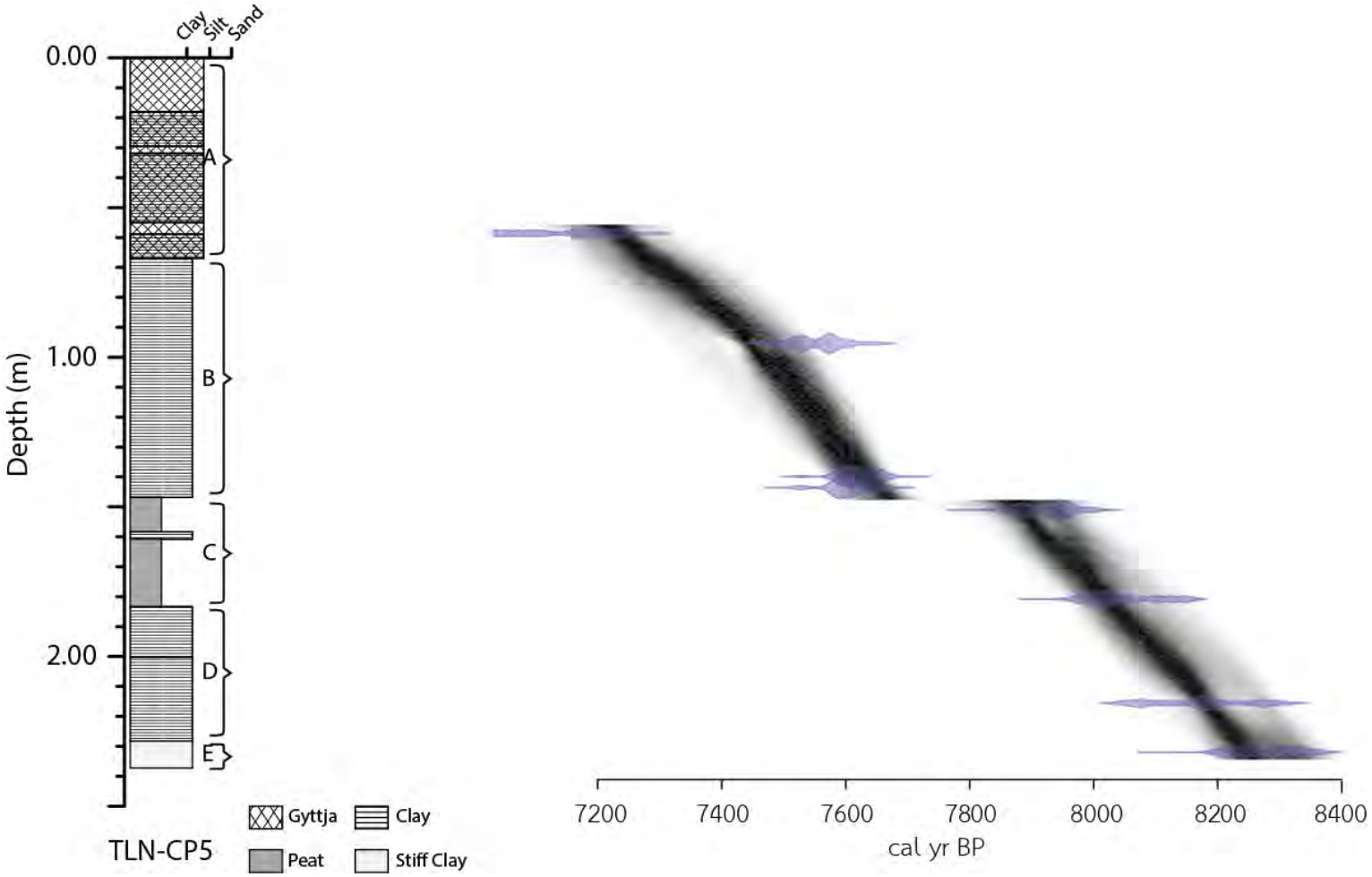

Figure 3.5 A comparison between the age-depth model and the lithostratigraphy.

CHAPTER IV

DISCUSSION AND CONLUSION

Sedimentology

As seen in Figure 3.1, the sedimentary sequence of five major sedimentary units, the lowermost unit, unit E: the stiff clay, is due to a high sea level above the area. Then, unit D: clay accumulated due to the regressive because it contains more organic material. After that, unit C's accumulation shows the lowest sea level since lots of plant are allowed to grow. Then, unit B, clay with detrital organic material, accumulated due to a transgression because the organic material is decreased. Finally, unit A, gyttja clay, accumulated due to a regression because of the decreasing of organic material.

Palynology

As seen in Figure 4.2, all pollen assemblage can be categorized into 3 environments: mangrove, back mangrove, and freshwater swamp. Since these pollen type can inform us which environment these pollen deposit, we can assess the sea level from them. Firstly, there are no pollen deposit before 8265 – 8086 cal yr. BP. This means the sea level was high and was covering the area. Secondly, there is an increase in mangrove pollens, and drop with an increase in transition pollens. This means there was a regression before 8145 – 7979 cal yr. BP. Thirdly, there is a decrease in transition pollen and an increase in mangrove pollens. This means there was a transgression after 8145 – 7979 cal yr. BP. Then, the sea level remained constant for a moment and then start to fall due to an increasing in terrestrial pollens and a decreasing in mangrove pollens after 7383 – 7156 cal yr. BP.

After 7315 – 7081 cal yr. BP at 56 cm from the top of the core, there is no chronological data. Although the sea level was lowering after 7383 – 7156 cal yr. BP, it slightly rose for a short period regarding to increasing mangrove pollens and decreasing terrestrial pollens between 20 and 30 cm from the top of the core. Finally, the sea level started to fall again due to a decreasing mangrove pollens and an increasing in terrestrial pollens.

Conclusion

As seen in Figure 4.3, if we combine all data (sedimentology, LOI, PSD, palynology, and ages), a sea level change model can be reconstructed as follows:

1. Regression 1 (before 8145 – 7979 cal BP)

The sea level was high enough to cover the study area. The environment should be a beach zone since the core cannot drilled deeper because it reached the sand layer. Then the sea level started to fall. The environment became a mangrove. But, since the sea level continued to fall, the mangrove also disappeared, and a transition environment was found instead at 8145 – 7979 cal BP.

2. Transgression (8145 – 7979 cal BP to 7383 – 7156 cal BP)

Since 8145 – 7979 cal BP, the sea level began to rise to a height where mangrove environment was still existed. So, the sea level may had been stayed stable between 7980 – 7787 cal BP to 7383 – 7156 cal BP.

3. Regression 2 (7383 – 7156 cal BP to recent)

Since 7383 – 7156 cal BP, the sea level began to fall again. Beside the regression, due to an increase in freshwater swamp pollen, there should be a freshwater run-off into the lake. At 30 cm deeps (there is no geochronological data for this sequence), There is an increase in mangrove pollen and a decrease in freshwater

swamp pollen. This should be due to a decrease in freshwater run-off, not the sea level change. So, the sea level should be falling as previously description.

Comparing to previous works, Horton et al. (2005) and Chaimanee et al. (1986), this study has information on the event before the transgression, whereas the others does not (Figure 4.4). This study shows that there is a regression (regression 1) before the transgression. The slightly difference in the time when events occur is because the difference in the characteristic of the study area of each studies. The core which was studied by Chaimanee et al. (1986) was collect far inland compared to this study. As for Horton et al. (2005), their core was collect from the land in the northeast of the lake, not in the lake.

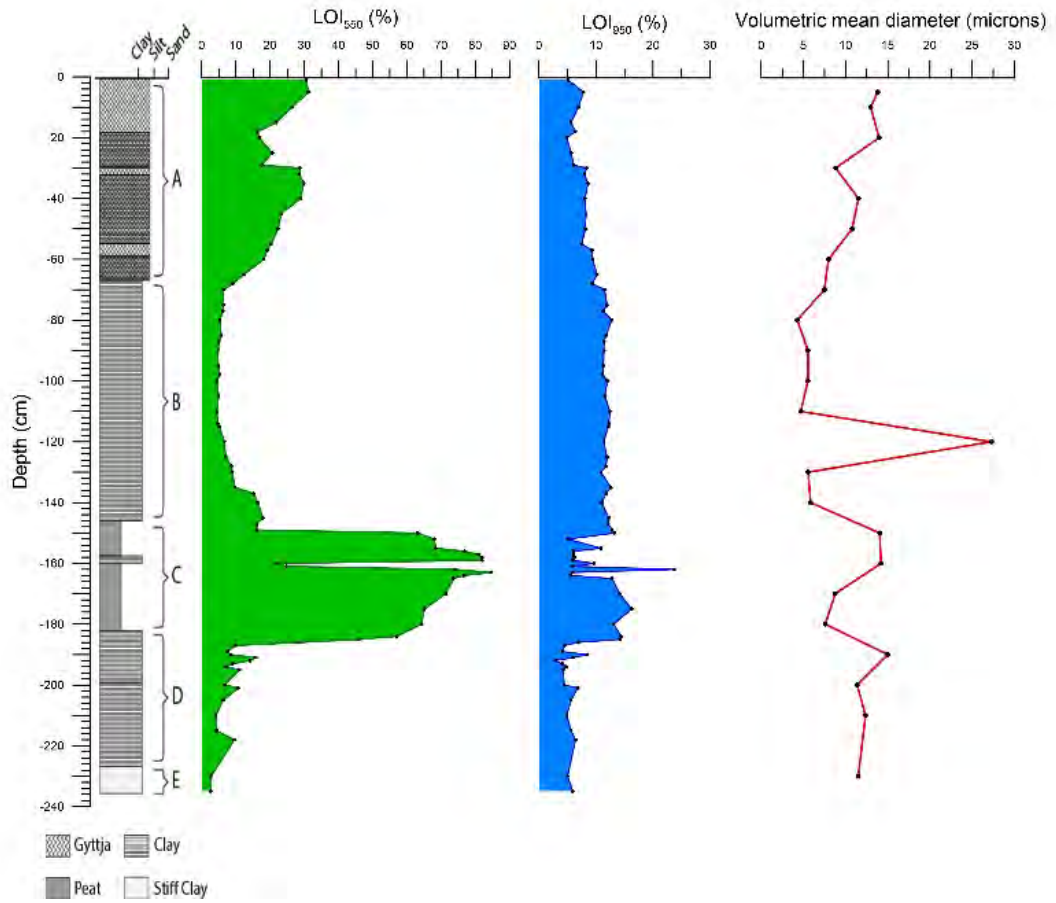

Figure 4.1 A graph compares lithostratigraphy, organic material (%), $CaCO_3$ (%), andparticle diameter with depth and calendar age.

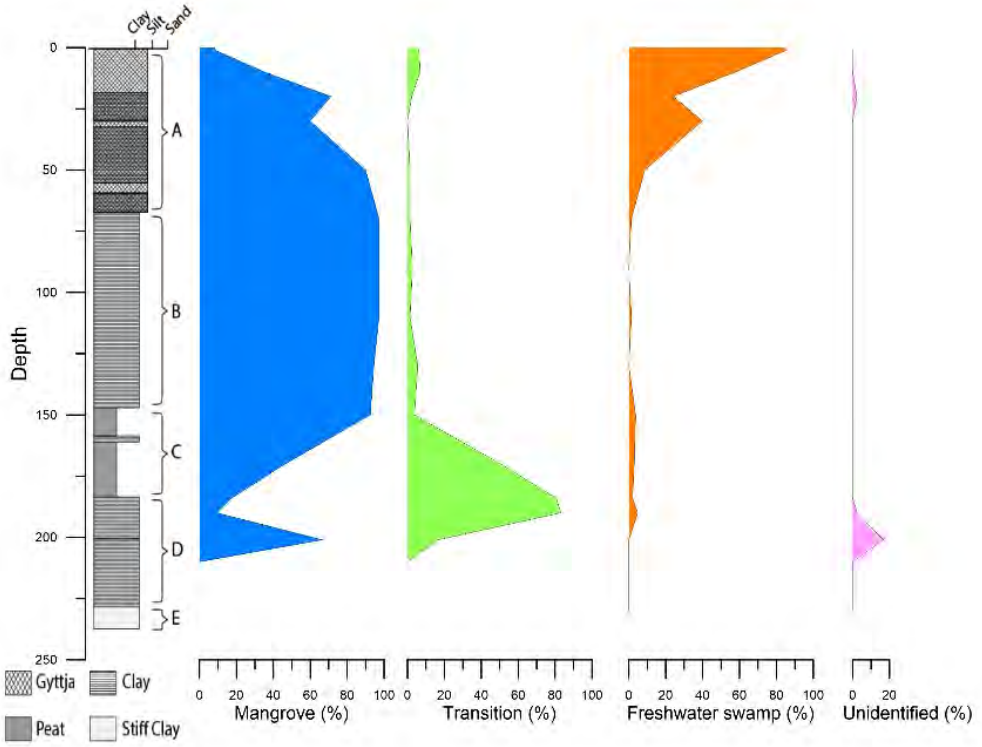

Figure 4.2 A graph compares mangrove lithostratigraphy, mangrove pollen (%), transition pollen (%), terrestrial pollen (%), and unidentified pollen (%) with depth and calendar age (Nudnara, in press)

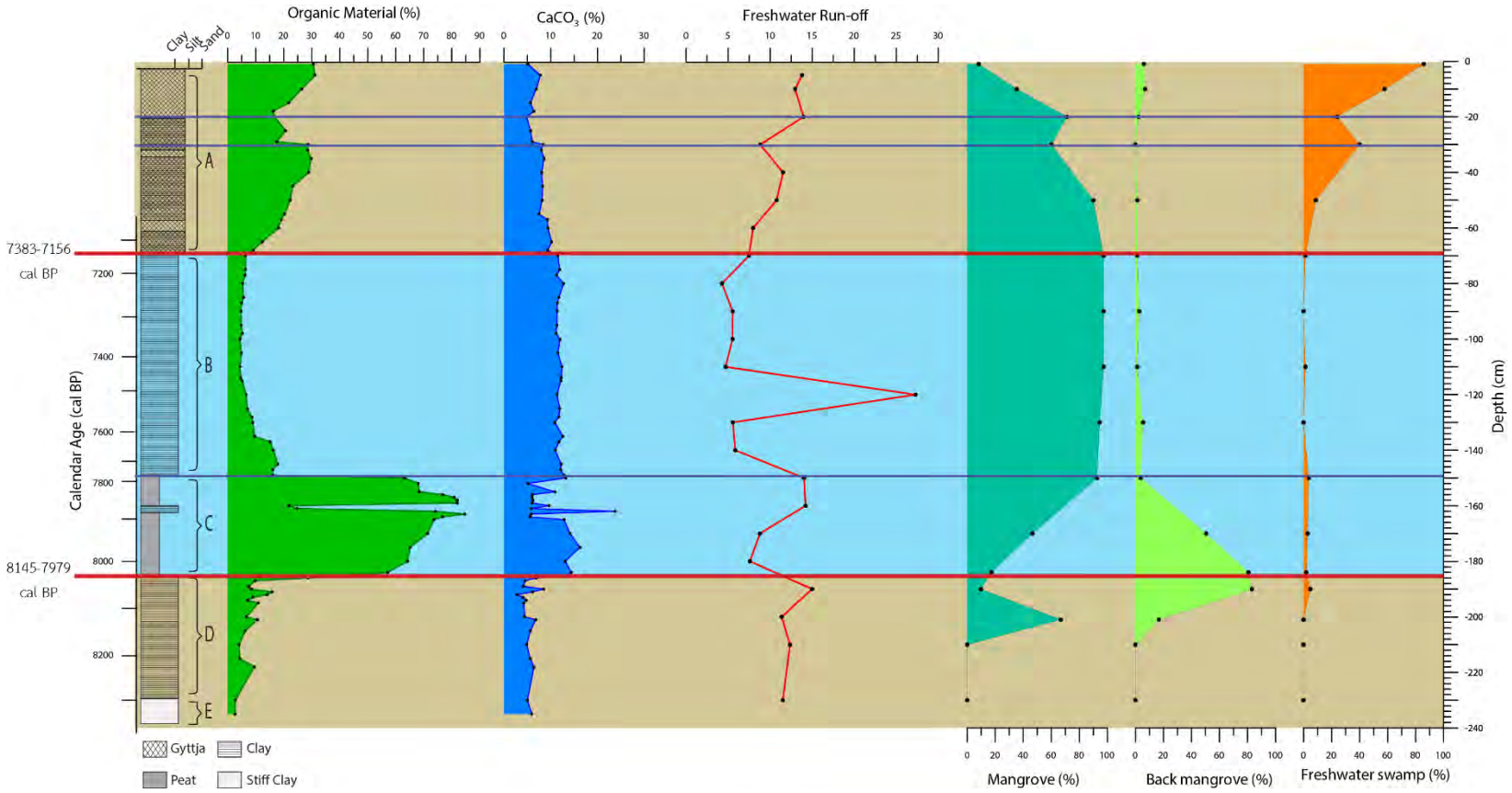

Figure 4.3 A graph compares Figure 4.1 and 4.2. A red line divided sedimentary sequence into 4 sections due to all information. The lowermost section is a regression. The upper section is a transgression. The upper section is a regression. And The uppermost section is a regression and influence of freshwater run-off into the lake.

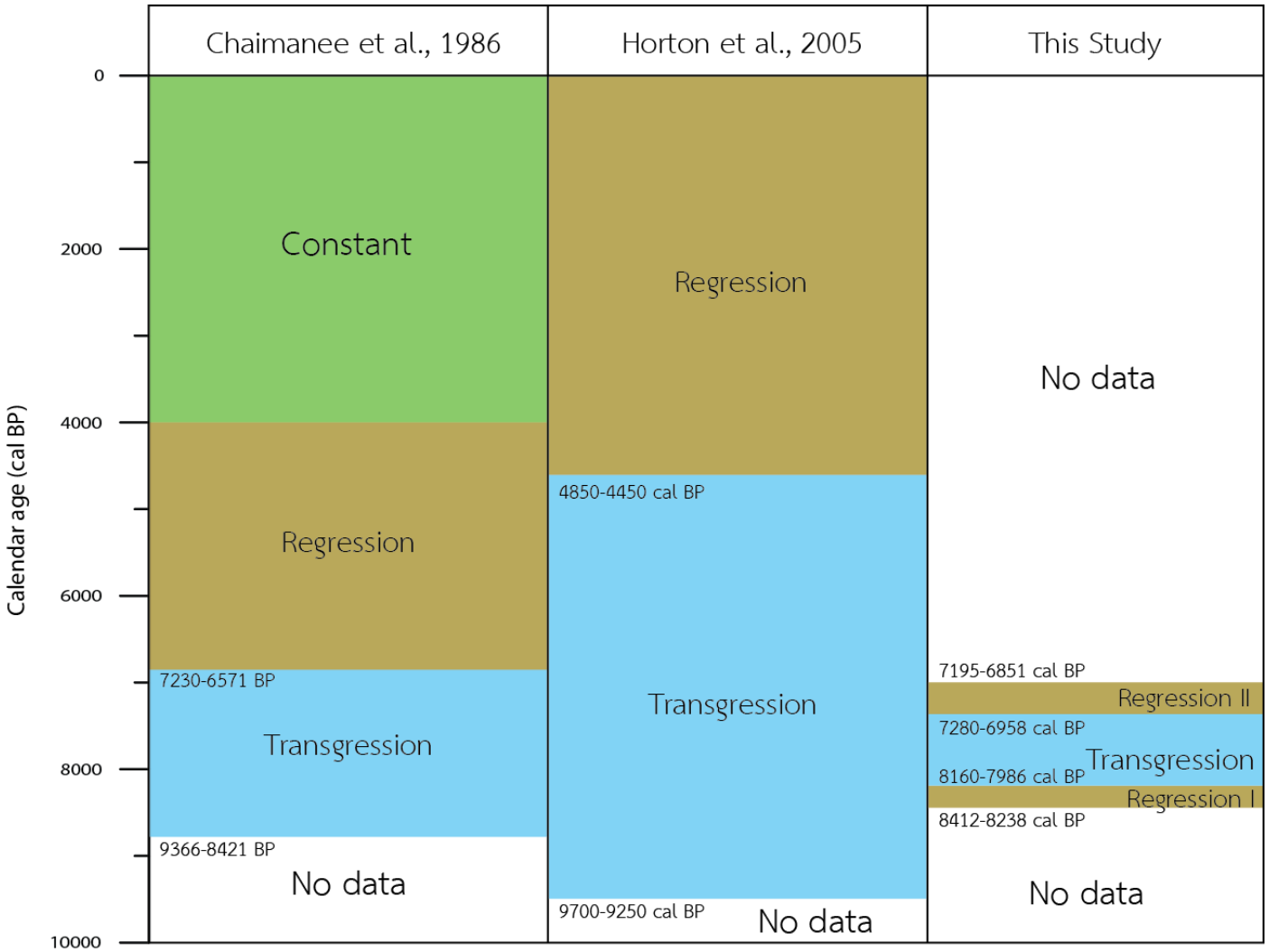

Figure 4.4 A comparison between this study, Horton et al. (2005), and Chaimanee et al. (1986).

REFERENCE

กองทัพไทย, กองบัญชาการ. กรมแผนที่ทหาร. 2542. อำเภอชะอวด [แผนที่].

ทรัพยากรธรรมชาติและสิ่งแวดล้อม, กระทรวง. กรมทรัพยากรธรณี. 2550. ธรณีวิทยาประเทศไทย. พิมพ์ครั้งที่ 2. กรุงเทพมหานคร: โรงพิมพ์ดอกเบี้ย.

นิรันดร์ ชัยมณี, เสริมศักดิ์ ติยพันธ์ และ นราเมศวร ธีระรังสิกุล. 2529. ธรณีวิทยาระวางอำเภอชะอวด และระวางระโนด. รายงานการสำรวจธรณีวิทยา. 45 หน้า.

Beuselinnck, L.; Govers, G.; Poesen, J.; Degraer, G.; and Froyen, L. 1998. Grain-size analysis by laser diffractometry: comparison with the sieve-pipette method. Catena. 32: 193-208.

Björck, S. and WohlFarth, B. 2002. ^{14}C chronostratigraphic techniques in paleolimnology. In W. M. Last and J. P. Smol (eds), Tracking Environmental Change Using Lake Sediments. Vol. 1. Basin analysis, coring, and chronological techniques, p.205-246. London: Springer.

Blaauw, M., and Christen, J. A. 2005. Radiocarbon peat chronologies and environmental change. Apply Statistic. 54, 4: 805-816.

Blaauw, M., and Christen, J. A. 2011. Flexible paleoclimate age-depth models using an autoregressive gamma process. Bayesian Analysis 6, 3: 457-474.

Blaauw, M. and Heegaard, E. 2012. Estimation of Age-Depth Relationships. In H. J. B. Birks; A. F. Lotter; S. Juggings; and J. P. Smol (eds), Tracking Environmental Change Using Lake Sediments. Vol. 5. Data handling and numerical techniques, p.379-414. London: Springer.

Brock, F.; Higham, T., Ditchfield, P.; and Ramsey, C. B. 2010. Current pretreatment methods for AMS radiocarbon dating at the Ocford Radiocarbon Accelerator Unit (ORAU). Radiocarbon. 52, 1: 103-112.

Christen, J. A. 1994. Bayesian interpretation of ^{14}C results. Doctoral dissertation. University of Nottingham. cited in Blaauw, M., and Christen, J. A. 2005. Radiocarbon peat chronologies and environmental change. Apply Statistic. 54, 4: 805-816.

Heiri, O.; Lotter, A. F.; and Lemcke, G. 2001. Loss on ignition as a method for estimating organic and carbonate content in sediments: reproducibility and comparability of results. Journal of Paleolimnology. 25: 101-110.

Horiba Instrument. n.d. A guidebook to particle size analysis. 29 pp.

Horton, B. P., Gibbard, P. L., Milne, G. M., Morley, R. J., Purintavaragul, C., and Stargardt, J. M. 2005. Holocene sea levels and palaeoenvironments, Malay-Thai peninsula, Southeast Asia. The Holocene. 15, 8: 1199-1213.

Matthews, J. A., ed. 2014. Encyclopedia of environmental change. Vol. 1. London: SAGE Publications.

Matthews, J. A., ed. 2014. Encyclopedia of environmental change. Vol. 2. London: SAGE Publications.

Matthews, J. A., ed. 2014. Encyclopedia of environmental change. Vol. 3. London: SAGE Publications.

Ministry of Information and Communication Technology, Thai Meteorological Department. 2015. The climate of Thailand. 7 pp.

Nudnara, W. in press. Paleoenvironmental reconstruction based on palynology in Thale Noi, Changwat Phatthalung. Senior project. Department of Geology, Faculty of Science, Chulalongkorn University.

Reimer, P. J., Bard, E., Bayliss, A., Beck, J. W., Blackwell, P. G., Ramsey, C. B., Buck, C. E., Cheng, H., Edwards, R. L., Friedrich, M., Grootes, P. M., Guilderson, T. P., Haflidason, H., Hajdas, I., Hatté, C., Heaton, T. J., Hoffmann, D. L., Hogg, A. G., Hughen, K. A., Kaiser, K. F., Kromer, B., Manning, S. W., Niu, M., Reimer, R. W., Richards, D. A., Scott, E. M., Southon, J. R., Staff, R. A., Turney, C. S. M., Plicht, J. van der. 2013. Intcal13 and Marine13 radiocarbon age calibration curves 0-50,000 years cal BP. Radiocarbon. 55, 4: 1869-1887.

Rowell, D. L. 1994. Soil science: methods and application. NY: Routledge.

Stargardt, J. M. 1983. Satingpra I, the environment and economic archaeology of South Thailand. Oxford and Singapore: British Archaeological Report (BAR) and Institute of Southeast Asian Studies (ISEAS), 332 pp. cited in Horton, B. P., Gibbard, P. L., Milne, G. M., Morley, R. J., Purintavaragul, C., and Stargardt, J. M. 2005. Holocene sea levels and palaeoenvironments, Malay-Thai peninsula, Southeast Asia. The Holocene. 15, 8: 1199-1213.

Stuiver, M., and Pollach, H. A. 1977. Discussion of reporting ^{14}C data. Radiocarbon. 19: 355-363. cited in Blaauw, M., and Christen, J. A. 2005. Radiocarbon peat chronologies and environmental change. Apply Statistic. 54, 4: 805-816.

Yoojam, N. 2015. Paleoenvironmatal reconstruction based on lake sediments from Thale Noi, Changwat Phatthalung. Senior project. Department of Geology, Faculty of Science, Chulalongkorn University.

APPENDICES

APPENDIX A

Table 1 Core location

Names	Latitude	Longtitude	UTM (WGS84)		Water Depth	Core Depth
			X	Y	(cm)	(cm)
TLN-CP3	7°47’23”	100°07’40”	624351	861217	150	234
TLN-CP4	7°47’11”	100°09’00”	626802	860855	200	184
TLN-CP5	7°47’15”	100°08’23”	625668	860975	150	238
TLN-CP7	7°47’03”	100°09’60”	628641	860615	150	292
TLN-CP8	7°47’34”	100°09’04”	626923	861562	200	168
TLN-CP9	7°48’05”	100°09’07”	627012	862515	200	231
TLN-CP10	7°46’38”	100°09’07”	627019	859842	200	143
TLN-CP11	7°47’06”	100°09’32”	627783	860704	200	139
TN-CP3	7°45’	100°10'	62865	85684	-	-

*Note: core TN-CP3 in the bottom of Table 1 is the core from Horton et al. (2005)

APPENDIX B

Loss on Ignition

Heiri et al. (2001) performed tests to assess possible bias when performing the loss on ignition (LOI) method to estimate organic material and carbonate content of lake sediments. At the same temperature, results show the relationship between the weight loss and both sample size and exposure time. The principle of this procedure is to compare the weight loss of samples at each temperature to the initial sample weight as equation 1.1 and 1.2. Finally, they conclude that an exposure to at least 4 hours at 550 °C for estimating organic material, and an exposure to at least 2 hours at 950 °C for estimating carbonate content. In addition, at 950 °C, carbonate content ($CaCO_3$) are combust to CO2, leaving CaO behind. So, the weight loss of CO_2 at 950 °C must be calculate back to $CaCO_3$ as equation 1.3, and 1.4

Equation 1.1 $$LOI_{550} = \frac{DW_{105} - DW_{550}}{DW_{105}} \, x \, 100$$

Equation 1.2 $$LOI_{950} = \frac{DW_{550} - DW_{950}}{DW_{105}} \, x \, 100$$

Equation 1.3 $$CaCO3 \longrightarrow CaO + CO_2$$

Equation 1.4 $$\frac{CaCO_3}{CO_2} = \frac{MW_{CaCO_3}}{MW_{CO_2}} = \frac{100.086 \, g/mol}{44.009 \, g/mol} = 2.27422$$

Where DW_t = Dry weight of samples at t °C (g)

MW = Molecular weight (g/mol)

LOI_t = weight loss on ignition at t °C (%)

Table 2 Raw LOI Results – 79 samples with color scale

No.	Depth (cm)	DW_{105} (g)	DW_{550} (g)	DW_{950} (g)	OM (%)	$CaCO_3$ (%)
1	0-1	0.134	0.093	0.090	30.6%	7.3%
5	4-5	0.321	0.221	0.210	31.2%	11.3%
10	9-10	0.197	0.145	0.139	26.4%	9.4%
15	14-15	0.767	0.600	0.581	21.8%	7.2%
18	17-18	0.818	0.685	0.662	16.3%	7.6%
20	19-20	0.517	0.430	0.419	16.8%	5.8%
25	24-25	0.640	0.508	0.492	20.6%	7.2%
29	28-29	0.751	0.619	0.599	17.6%	7.3%
30	29-30	0.380	0.271	0.257	28.7%	11.7%
32	31-32	0.683	0.488	0.464	28.6%	11.2%
35	34-35	0.768	0.539	0.510	29.8%	12.2%
40	39-40	0.647	0.460	0.437	28.9%	11.4%
45	44-45	0.826	0.634	0.604	23.2%	10.8%
50	49-50	0.641	0.498	0.475	22.3%	10.5%
55	54-55	0.819	0.653	0.626	20.3%	9.4%
57	56-57	1.024	0.828	0.786	19.1%	11.5%
60	59-60	0.822	0.673	0.639	18.1%	11.5%
65	64-65	1.607	1.409	1.337	12.3%	11.6%
68	67-68	1.461	1.328	1.268	9.1%	10.3%

Table 2 Raw LOI Results (continued)

No.	Depth (cm)	DW_{105} (g)	DW_{550} (g)	DW_{950} (g)	OM (%)	$CaCO_3$ (%)
70	69-70	1.026	0.961	0.909	6.3%	12.3%
75	74-75	1.354	1.268	1.197	6.4%	12.7%
77	76-77	2.142	2.009	1.903	6.2%	12.0%
80	79-80	0.944	0.894	0.841	5.3%	13.5%
85	84-85	1.915	1.806	1.707	5.7%	12.5%
87	86-87	1.236	1.174	1.112	5.0%	12.0%
90	89-90	1.679	1.599	1.515	4.8%	11.9%
95	94-95	1.968	1.873	1.775	4.8%	11.9%
98	97-98	1.712	1.622	1.538	5.3%	11.8%
100	99-100	0.890	0.851	0.804	4.4%	12.6%
105	104-105	2.087	1.984	1.878	4.9%	12.2%
110	109-110	1.042	0.996	0.939	4.4%	13.0%
114	113-114	1.669	1.591	1.501	4.7%	12.9%
115	114-115	1.942	1.841	1.737	5.2%	12.8%
120	119-120	0.881	0.823	0.779	6.6%	12.2%
125	124-125	1.846	1.716	1.619	7.0%	12.9%
128	127-128	1.721	1.571	1.482	8.7%	12.9%
130	129-130	1.066	0.971	0.920	8.9%	11.9%
135	134-135	1.118	1.010	0.948	9.7%	14.0%
137	136-137	1.351	1.146	1.076	15.2%	13.9%
140	139-140	0.849	0.710	0.669	16.4%	13.1%
145	144-145	0.798	0.655	0.612	17.9%	14.9%

Table 2 Raw LOI Results (continued)

No.	Depth (cm)	DW_{105} (g)	DW_{550} (g)	DW_{950} (g)	OM (%)	$CaCO_3$ (%)
147	146-147	0.769	0.645	0.604	16.1%	14.5%
149	148-149	1.063	0.892	0.832	16.1%	15.3%
150	149-150	0.258	0.095	0.080	63.2%	35.9%
152	151-152	0.178	0.057	0.053	68.0%	16.0%
155	154-155	0.396	0.125	0.106	68.4%	34.6%
156	155-156	0.112	0.026	0.023	76.8%	26.2%
157	156-157	0.188	0.036	0.031	80.9%	31.6%
158	157-158	0.183	0.033	0.028	82.0%	34.5%
159	158-159	0.266	0.048	0.041	82.0%	33.2%
160	159-160	0.779	0.608	0.575	22.0%	12.3%
161	160-161	0.584	0.439	0.424	24.8%	7.8%
162	161-162	0.220	0.057	0.034	74.1%	91.8%
163	162-163	0.156	0.024	0.020	84.6%	37.9%
164	163-164	0.244	0.057	0.051	76.6%	23.9%
165	164-165	0.496	0.131	0.103	73.6%	48.6%
170	169-170	0.370	0.106	0.083	71.4%	49.3%
175	174-175	0.461	0.161	0.128	65.1%	46.6%
180	179-180	0.347	0.124	0.104	64.3%	36.7%
184	183-184	0.489	0.210	0.179	57.1%	33.6%
185	184-185	0.592	0.320	0.283	45.9%	26.3%
186	185-186	0.596	0.425	0.407	28.7%	9.6%

Table 2 Raw LOI Results (continued)

No.	Depth (cm)	DW_{105} (g)	DW_{550} (g)	DW_{950} (g)	OM (%)	$CaCO_3$ (%)
187	186-187	0.953	0.859	0.840	9.9%	5.0%
189	188-189	1.097	1.014	0.994	7.6%	4.5%
190	189-190	1.178	1.078	1.034	8.5%	9.3%
191	190-191	1.232	1.037	1.004	15.8%	7.2%
192	191-192	1.039	0.892	0.879	14.1%	3.3%
193	192-193	2.569	2.339	2.293	9.0%	4.5%
194	193-194	2.727	2.532	2.475	7.2%	5.1%
195	194-195	1.495	1.331	1.303	11.0%	4.8%
200	199-200	1.232	1.150	1.126	6.7%	4.7%
201	200-201	1.334	1.192	1.152	10.6%	7.6%
205	204-205	2.539	2.380	2.317	6.3%	6.0%
210	209-210	3.084	2.958	2.892	4.1%	5.1%
215	214-215	2.554	2.444	2.381	4.3%	5.9%
218	217-218	1.631	1.476	1.430	9.5%	7.1%
230	229-230	2.357	2.292	2.240	2.8%	5.2%
235	234-235	3.020	2.939	2.860	2.7%	6.1%

APPENDIX C

Particle size distribution

There are several ways to analyze the particle size distribution, for examples, the sieve-pipette method, the hydrometer method, and the laser diffraction. The sieve-pipette method (sometimes a hydrometer is used instead of a pipette), which is known for conventional technique, are based on Stroke's law. The law states that denser particles sink further than less dense particles. The coarse fractions are determined by the sieve method, and the fine fractions are determined by the pipette method. Anyway, both methods have a lower reproducibility than the laser diffraction method (Beuselinck et al., 1998: 193). The laser diffraction method is based on laser diffraction technique. When light travel through suspended particles, the light will be diffracted. The diffraction depends on the diameter of the particle, and the frequency of the light. There are 2 theories on laser diffraction, Mie's scattering theory, and Fraunhofer' theory. The laser particle sizer at Scienctific and Technological Research Equipment Centre (STREC), Malvern Mastersizer 3000, is based on Mie's scattering theory. Mie's theory considers these parameter: the wave range of the light source, refractive index of the particle and the medium, which provides more accuracy and precision data than Fraunhofer's.

If samples were all spherical particle, the result would come out as a single number, the diameter. However, most particles we find in the world are not a sphere. So, as seen in Figure 1.4, non-spherical particle can be described using multiple number (Horiba instrument, n.d.). Since there are a lot of value to describe the result, both the central point and the distribution width must be report.

2.1 Central point

2.1.1 Mean: There are 3 means depend on the basis of the distribution (number, surface, volume). They are all shown in Equation 1.5, 1.6, and 1.7

2.1.1.1. Arithmetic or number mean (D[1,0])

2.1.1.2. Surface mean (D[3,2])

2.1.1.3. Volumetric mean (D[4,3])

This is the most appropriate central value for the study.

2.1.2 Median: Median (D_{50}) is a value where half of the population is above this value, and the other half is below the value.

2.1.3 Mode: Mode is the value which has the most frequency in the distribution.

2.2 Distribution width

This is described by SPAN, as shown in Equation 1.8.

Equation 1.5 $$D[1,0] = \frac{\sum_1^i D_i}{n}$$

Equation 1.6 $$D[3,2] = \frac{\sum_1^i D_i^3}{\sum_1^i D_i^2}$$

Equation 1.7 $$D[4,3] = \frac{\sum_1^i D_i^4}{\sum_1^i D_i^3}$$

Equation 1.8 $$Span = \frac{D_{90} - D_{10}}{D_{50}}$$

Where:

- D[1,0] = arithmetic or number mean diameter
- D[3,2] = surface mean diameter
- D[4,3] = the mean diameter over volume
- D_i = the diameter of the ith particle
- D_x = the diameter where x% of the population have less diameter

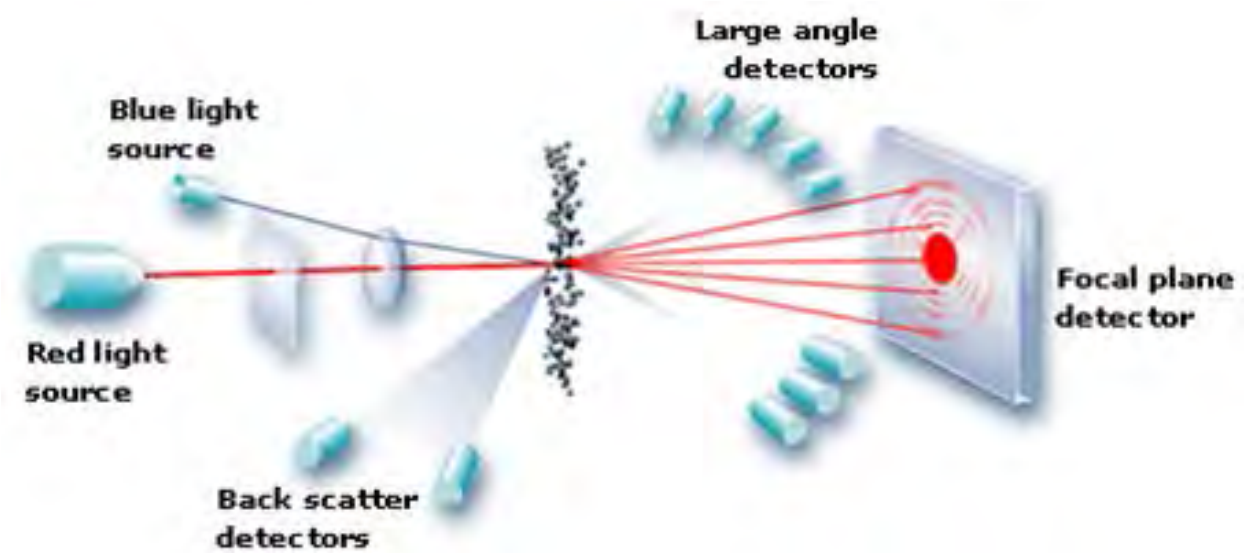

Figure 5.1 The function of a laser particle sizer (Horiba instrument, n.d.)

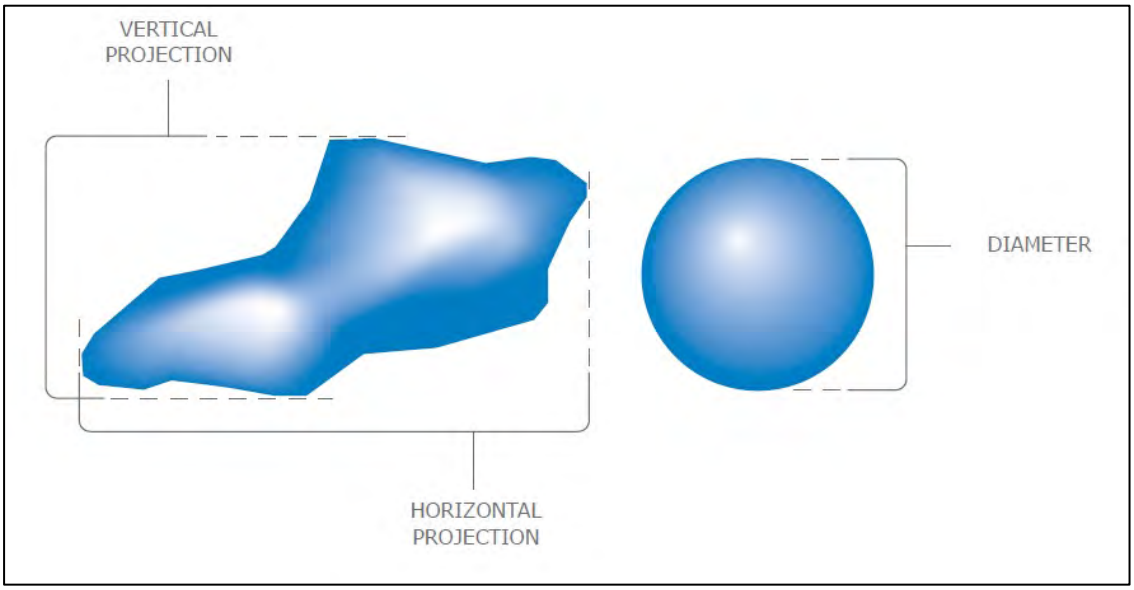

Figure 5.2 The shape of the particle (Horiba instrument, n.d.)

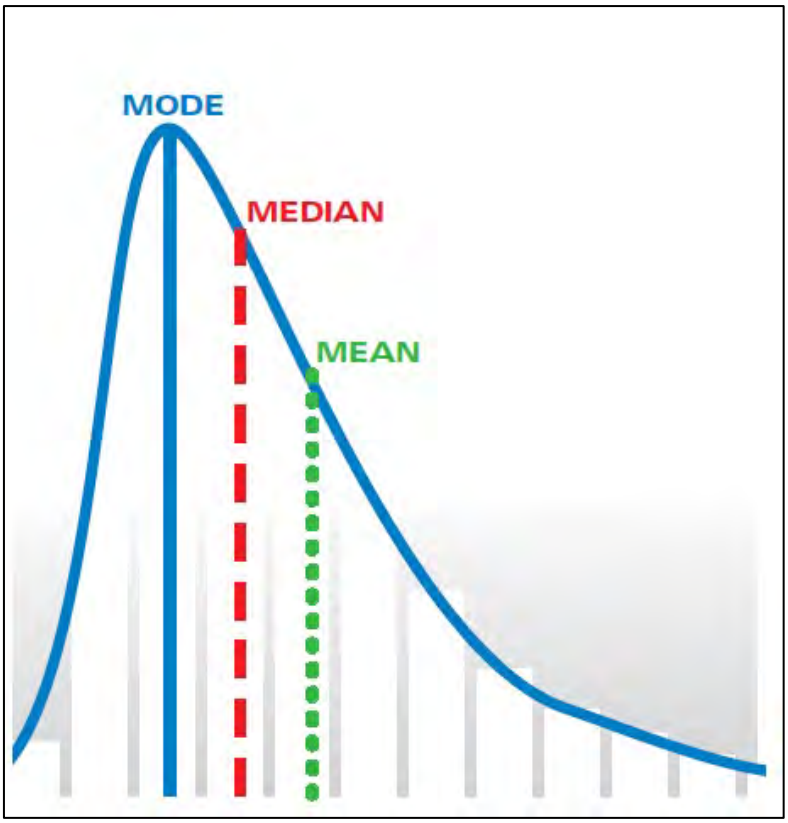

Figure 5.3 Mode, median, and mean of a non-symmetrical distribution (Horiba instrument, n.d.)

Table 3 Raw particle size distribution data

Depth (cm)	D_{10} (µm)	D_{50} (µm)	D_{90} (µm)	D[4,3] (µm)	D[3,2] (µm)	Laser Obscuration (%)	Weighted Residual (%)	Span
4-5	1.38	8.47	28.50	13.70	3.83	11.11	1.15	3.20
4-5	1.38	8.51	29.10	14.10	3.84	11.10	1.14	3.26
4-5	1.38	8.49	28.60	13.60	3.83	11.10	1.14	3.21
9-10	1.35	9.05	26.10	12.90	3.86	18.71	1.04	2.73
9-10	1.34	9.09	26.30	13.00	3.85	18.64	1.04	2.75
9-10	1.32	9.09	26.30	13.00	3.83	18.65	1.05	2.75
19-20	1.75	10.60	26.20	13.90	4.56	18.34	0.93	2.31
19-20	1.74	10.70	26.20	14.00	4.55	18.26	0.93	2.29
19-20	1.71	10.70	26.20	14.00	4.53	18.13	0.93	2.29
29-30	1.48	6.68	19.40	8.89	3.64	21.23	1.26	2.68
29-30	1.43	6.56	19.30	8.80	3.57	21.06	1.28	2.72
29-30	1.40	6.47	19.20	8.73	3.52	20.94	1.29	2.75
39-40	0.92	4.98	22.00	11.50	2.69	14.84	1.51	4.23
39-40	0.91	4.96	22.20	11.70	2.67	14.81	1.51	4.29
39-40	0.90	4.89	21.90	11.40	2.64	14.76	1.53	4.29
49-50	1.16	5.66	20.40	10.80	3.13	26.02	1.24	3.40
49-50	1.14	5.63	20.40	10.70	3.11	26.14	1.24	3.42

Table 3 Raw particle size distribution data (continued)

Depth (cm)	D_{10} (µm)	D_{50} (µm)	D_{90} (µm)	D[4,3] (µm)	D[3,2] (µm)	Laser Obscuration (%)	Weighted Residual (%)	Span
49-50	1.12	5.59	20.50	10.80	3.08	26.01	1.25	3.47
59-60	1.06	5.57	18.20	7.98	2.98	24.69	1.30	3.08
59-60	1.05	5.54	18.20	7.96	2.96	24.59	1.31	3.10
59-60	1.04	5.52	18.30	7.96	2.94	24.54	1.32	3.13
69-70	1.09	5.67	16.30	7.48	3.03	28.92	1.24	2.68
69-70	1.08	5.65	16.30	7.46	3.02	28.93	1.24	2.69
69-70	1.08	5.66	16.30	7.47	3.02	28.99	1.24	2.69
79-80	0.81	3.04	9.19	4.26	2.00	24.82	1.84	2.76
79-80	0.81	3.05	9.19	4.27	2.00	24.87	1.84	2.75
79-80	0.81	3.04	9.20	4.26	2.00	24.92	1.85	2.76
89-90	1.28	4.14	11.80	5.63	2.88	18.78	1.54	2.54
89-90	1.28	4.11	11.60	5.55	2.87	18.82	1.55	2.51
89-90	1.27	4.06	11.30	5.45	2.84	18.92	1.57	2.47
99-100	1.09	4.09	11.80	5.54	2.67	29.19	1.46	2.62
99-100	1.08	4.08	11.80	5.52	2.66	29.24	1.46	2.63
99-100	1.08	4.07	11.70	5.50	2.65	29.29	1.46	2.61
109-110	0.78	3.19	10.20	4.69	1.98	12.40	2.05	2.95
109-110	0.78	3.21	10.20	4.69	1.98	12.47	2.05	2.94
109-110	0.78	3.22	10.20	4.69	1.99	12.49	2.06	2.93
119-120	1.03	3.52	14.10	28.70	2.49	23.04	1.58	3.71
119-120	1.03	3.51	14.00	26.50	2.48	23.05	1.58	3.70

Table 3 Raw particle size distribution data (continued)

Depth (cm)	D_{10} (µm)	D_{50} (µm)	D_{90} (µm)	D[4,3] (µm)	D[3,2] (µm)	Laser Obscuration (%)	Weighted Residual (%)	Span
119-120	1.03	3.49	14.10	26.70	2.48	23.06	1.58	3.74
129-130	0.94	3.65	12.20	5.53	2.39	16.95	1.74	3.08
129-130	0.94	3.61	12.20	5.54	2.37	16.98	1.78	3.12
129-130	0.93	3.57	12.30	5.59	2.36	17.02	1.82	3.18
139-140	0.97	4.00	13.20	5.92	2.53	25.58	1.54	3.06
139-140	0.96	3.94	13.00	5.84	2.50	25.61	1.56	3.06
139-140	0.95	3.88	12.80	5.78	2.47	25.62	1.58	3.05
159-160	1.69	7.59	27.80	13.80	4.09	17.70	1.06	3.44
159-160	1.65	7.44	28.10	15.70	4.02	17.85	1.07	3.56
159-160	1.59	7.17	26.90	13.10	3.91	17.98	1.09	3.53
169-170	0.69	4.36	22.10	8.82	2.01	5.01	1.91	4.91
169-170	0.69	4.33	22.40	8.89	1.99	4.98	1.88	5.01
169-170	0.68	4.18	21.90	8.61	1.95	4.94	1.90	5.08
179-180	0.72	3.72	18.60	7.47	2.00	21.07	1.61	4.81
179-180	0.72	3.72	18.90	7.59	2.00	21.03	1.61	4.89
179-180	0.72	3.70	19.10	7.70	1.99	21.00	1.62	4.97
189-190	1.03	4.95	28.70	15.00	2.86	26.00	1.26	5.59
189-190	1.03	4.93	28.80	14.90	2.85	26.02	1.27	5.63
189-190	1.03	4.94	29.20	15.10	2.85	26.05	1.27	5.70
199-200	1.17	7.21	27.60	11.40	3.40	18.74	1.21	3.67
199-200	1.15	7.10	27.60	11.30	3.37	18.84	1.22	3.73

Table 3 Raw particle size distribution data (continued)

Depth (cm)	D_{10} (µm)	D_{50} (µm)	D_{90} (µm)	D[4,3] (µm)	D[3,2] (µm)	Laser Obscuration (%)	Weighted Residual (%)	Span
199-200	1.14	7.02	27.80	11.40	3.35	18.94	1.23	3.80
209-210	1.48	8.56	29.20	12.60	4.02	15.11	1.08	3.24
209-210	1.44	8.33	28.90	12.30	3.95	15.34	1.11	3.30
209-210	1.39	8.00	28.90	12.20	3.83	15.75	1.13	3.44
229-230	1.04	6.64	28.90	11.80	3.13	26.29	1.13	4.20
229-230	1.03	6.57	28.60	11.40	3.10	26.39	1.16	4.20
229-230	1.03	6.51	28.50	11.30	3.08	26.46	1.15	4.22
149-150	2.15	11.10	31.20	14.40	5.11	1.36	1.34	2.62
149-150	2.03	10.90	30.70	14.10	5.00	1.38	1.58	2.63
149-150	1.97	10.80	29.20	13.60	4.93	1.37	1.55	2.52

APPENDIX D

Radiocarbon dating and age-depth modelling

An accurate and Precise geochronology data is vital to paleolimnological studies because they can identify when the event occurs, making it easier to compare and correlate with the other (Blaauw and Heegaard, 2012)

^{14}C radiocarbon dating are most used for studying paleolimnology by examine the fraction between ^{14}C and ^{12}C ($^{14}C/^{12}C$) of the sample. When organism lives, the $^{14}C/^{12}C$ is constant. But, when it dies, since ^{14}C is a radioactive element, it decays, making the quantity of ^{14}C decreases. Thus, the fraction can be used to indicate ages of the sample.

Although the principle of indicating ages by using ^{14}C seems easy, it is not, since the radiocarbon age is not an absolute age because:

- Radiocarbon age comes with errors and uncertainties (Christen, 1994 cited in Blaauw and Christen, 2005)
- Contamination which affect the quantity of ^{14}C (Stuiver and Pollach, 1977 cited in Blaauw and Christen, 2005)
- Constraints in research budget or datable material can limit the number of dates (Blaauw and Christen, 2005)
- Because of the long- and short- term variations in atmospheric ^{14}C, the radiocarbon age must be calibrated to calendar age. But, the relationship between these two are not linear.

Problem No. 1 is a systematic error. No. 2 can be eliminated by choosing the right macrofossil to be dated. The rest problems can be eliminated by using these methods (Blaauw and Heegaard, 2012):

3.1 Basic Age Depth Modelling

consider only errors in each sample's age calculating. Assume that there is no relationship between each, and no systematic error.

3.2 Mixed-Effect Age-Depth Modelling

consider more possible error, including systematic error.

3.3 Bayesian Age-Depth Modelling

combines data with other available information during analysis.

3.3.1 Chronological Ordering – a method to find calendar ages from samples which already has ^{14}C ages. Basically, a calibration curve shows us that a single ^{14}C age can be calibrated into many calendar ages (Figure 1.6) But, if we consider more conditions. For example, information from sedimentary sequence that $\theta_1 > \theta_2 > \theta_3$ where θ is calendar age, and y_j is ^{14}C age, and the sedimentation rate must be positive. Information which conflict with above assumption can be ignore as a prior information (Figure 1.8). The calendar age retrieving from this method is a value with error equals to standard deviation. This is a conditional probability, and the calendar ages are posterior probability.

The above method can only have a specific ^{14}C of samples. The rest value, which are not dated, will be analyzed using statistical method, for example, linear interpolation (Figure 1.7), autoregressive gamma process, etc.

3.3.2 Wiggle Matching – a method to compare the ^{14}C ages fluctuation which are much closer in depth to a wiggle calibration curve. Then, it is overlaid to each other and directly calibrated into calendar age. Assuming the sedimentation rate is constant.

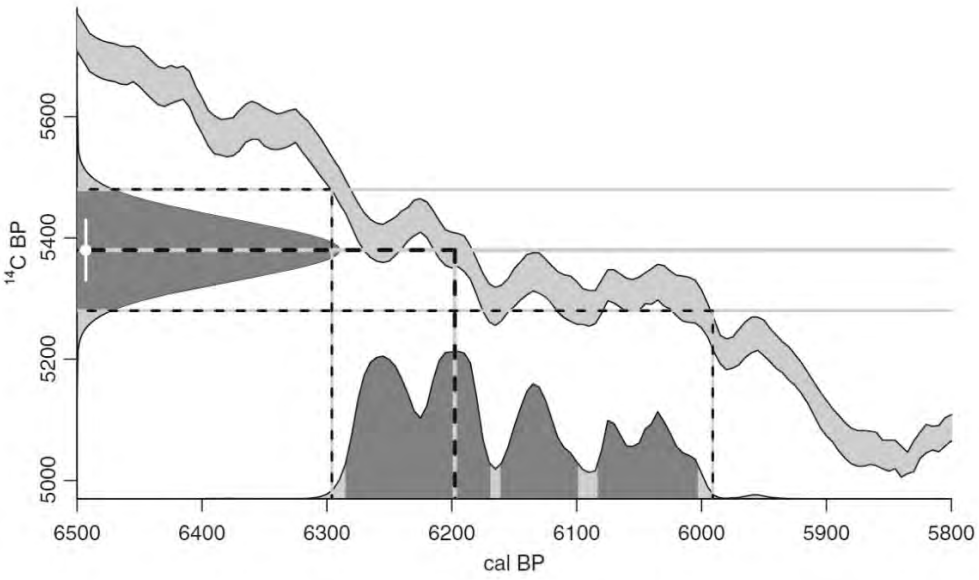

Figure 5.4 The relationship between ^{14}C age and calendar age. The histogram in the left side is a normal distribution of y_j ± 2 SD. The histogram below is a distribution of θ. The light grey area is a calibration curve, IntCal09, ± 2 SD (Blaauw and Heegaard, 2012).

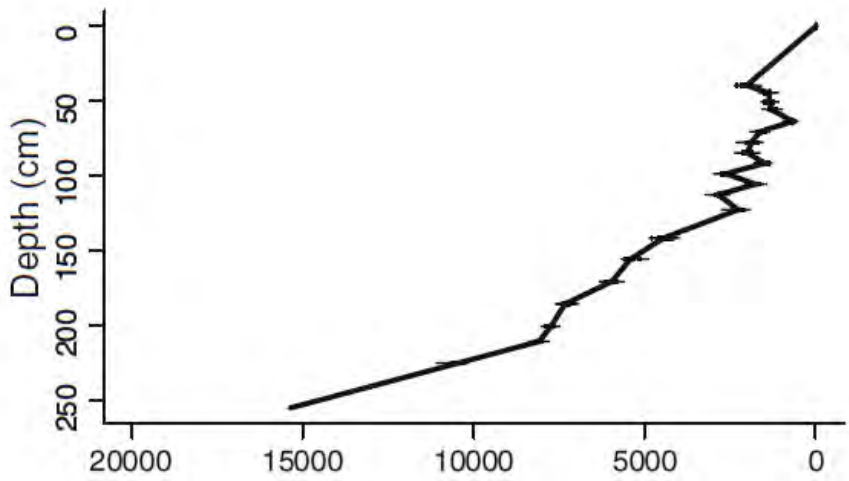

Figure 5.5 Linear interpolation method. The relationship between calendar age and depth of deposits. A tiny black dot and dash refer to θ_j ± 2 SD. Then, draw a straight line to connect each dot. From Blaauw and Heegaard (2012).

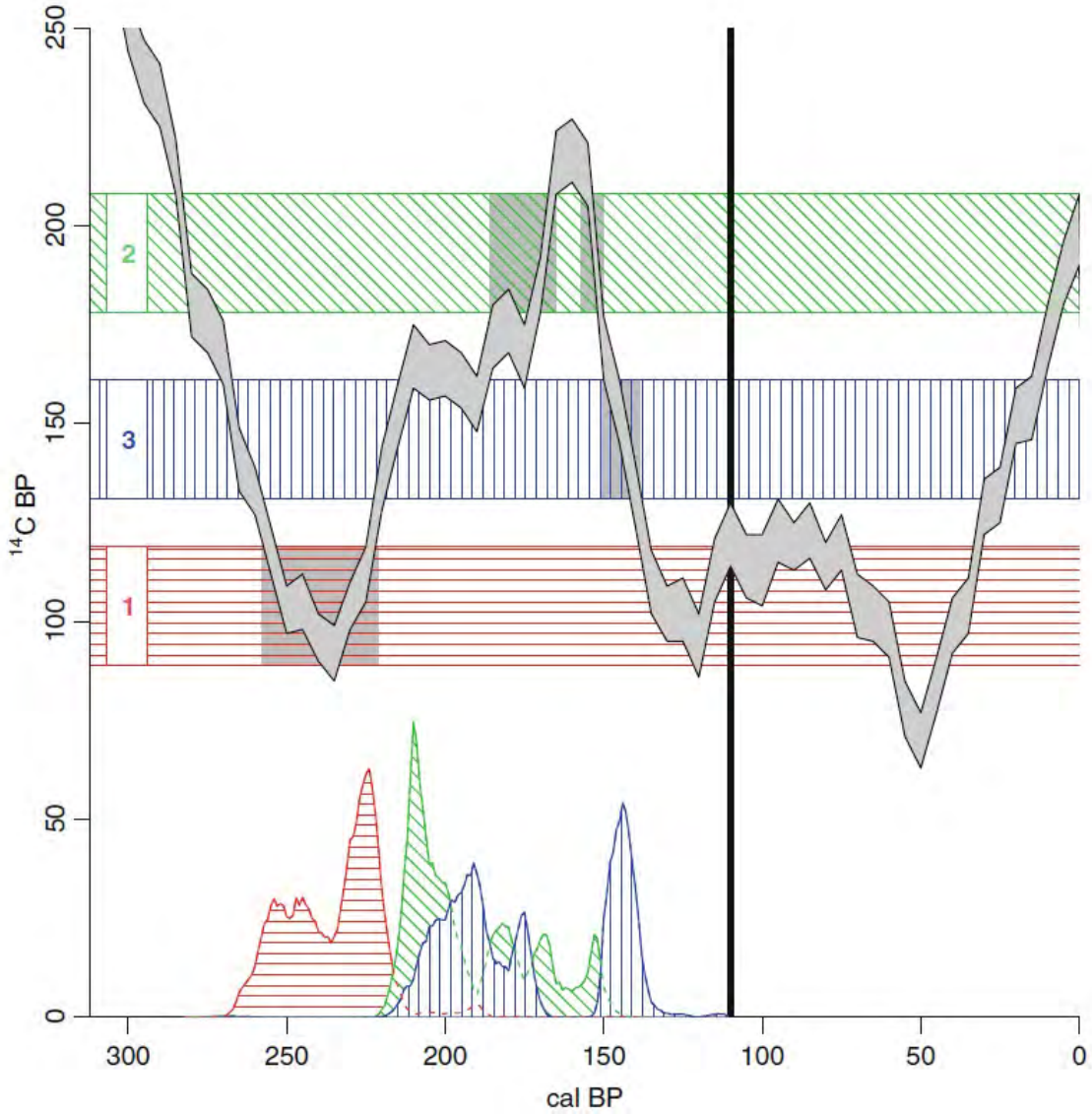

Figure 5.6 a chronological ordering Bayesian age-depth model when $\theta_1 > \theta_2 > \theta_3 >$ 110 cal BP. The light grey area is calibration cure ± 1 SD. The horizontal coloured stripes are y_1, y_2, y_3 ± 1 SD. It is noticed that information, which is emphasized by dark grey section, is consider only. The other are not considered because it conflicts with prior condition. From Ibbetson (2011), modified by Blaauw and Heegaard (2012).

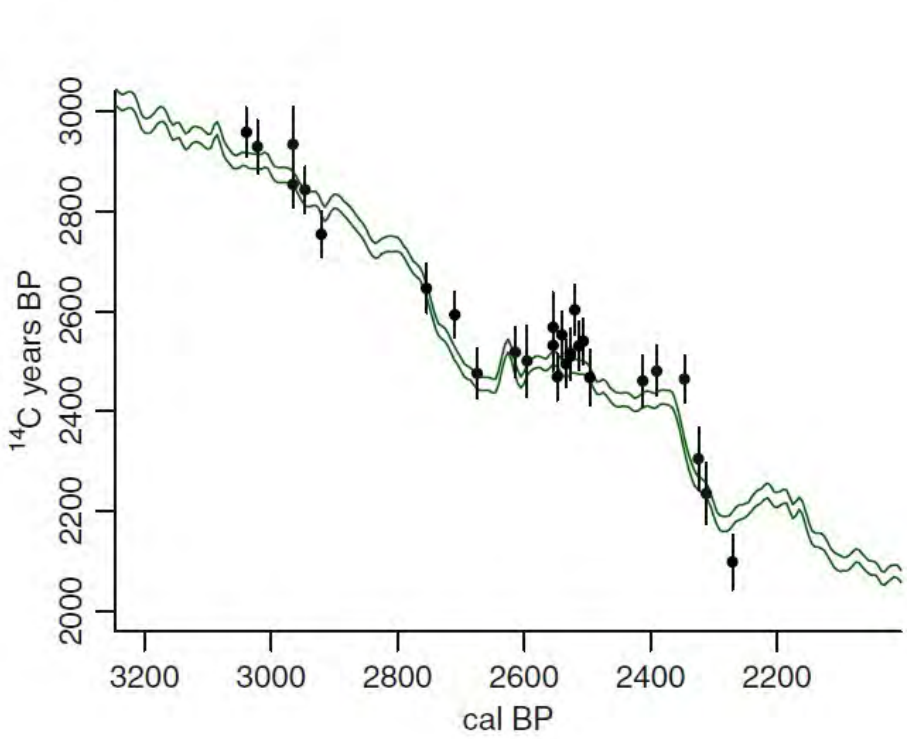

Figure 5.7 Wiggle-matching method. The green line is a calibration curve with error of 2 SD. Black dots and dashes are y_j. ± 2 SD. Both data is being compared to each other to retrieve calendar age. (Blaauw, and Heegaard, 2012).

Table 4 AMS ^{14}C Dating Results

Title	D-AMS ID	Depth (cm)	Represent	Material	Fraction of modern		^{14}C age	
					pMC	1SD error	BP	1SD error
TN-1	021771	8-13	Top A	leaves	104.36	0.30	Modern	
TN-9	021777	56-61	Bottom A	leaves	46.02	0.25	6234	44
TN-2	022509	93-98	Top B	leaves	43.48	0.20	6690	37
TN-3	021772	137.5-143	Bottom B	wood	43.08	0.18	6765	34
TN-11	022510	142-146	Bottom B	Leaves	43.19	0.19	6744	35
TN-8	021776	150-153	Top C	wood	41.30	0.18	7104	35
TN-4	021773	180-183	Bottom C	wood	40.71	0.18	7219	36
TN-5	021774	215-218	Bottom D	wood	40.01	0.17	7359	34
TN-6	021775	231-235	Bottom E	leaves, chalcoal	39.51	0.18	7460	37